πN and ηp deexcitation channels of the N^* and Δ baryonic resonances between 1470 and 1680 MeV

B. Tatischeff,[1,*] J. Yonnet,[1] M. Boivin,[2] M. P. Comets,[1] P. Courtat,[1] R. Gacougnolle,[1] Y. Le Bornec,[1] E. Loireleux,[1] M. MacCormick,[1] and F. Reide[1]

[1]*Institut de Physique Nucléaire, Universite Paris-Sud, CNRS/IN2P3, F-91406 Orsay Cedex, France*

[2]*Laboratoire National Saturne, CNRS/IN2P3, F-91191 Gif-sur-Yvette Cedex, France*

(Received 17 December 2004; published 21 September 2005)

Two reactions, $pp \to ppX$ and $pp \to p\pi^+X$, are used to study the $1.47 \leqslant M \leqslant 1.680$ GeV baryonic mass range. Three different final states are considered in the invariant masses: N^* or Δ^+, $n\pi^+$ or $p\pi^0$, and $p\eta$. The last two channels are defined by software cuts applied to the missing mass of the first reaction. Several narrow structures are extracted with widths $\sigma(\Gamma)$ varying between 3 and 9 MeV. Some structures are observed in one channel but not in another. Such nonobservation may be due either to the spectrometer momenta limits or to the physics (e.g., no such disintegration channel is allowed from the narrow state considered).

We tentatively conclude that the broad Particle Data Group (PDG) baryonic resonances—$N(1520)D_{13}$, $N(1535)S_{11}$, $\Delta(1600)P_{33}$, $N(1650)S_{11}$, and $N(1675)D_{15}$—are collective states built from several narrow and weakly excited resonances, each having a (much) smaller width than the one reported by PDG.

DOI: 10.1103/PhysRevC.72.034004 PACS number(s): 14.20.Gk, 13.30.Eg, 25.40.Ve

I. INTRODUCTION

For a number of years partial-wave analyses of baryonic resonances have been extensively developed using mainly $\pi N \to \pi N$, $\pi N \to \pi\pi N$, and $\gamma N \to \pi N$ reactions [1]. The study of the dynamics of the $\pi N \to \pi\pi N$ reaction [2] is also useful for improving our knowledge about meson production, as well as our knowledge of the baryonic resonances. These resonances have also been studied with $pp \to pN^*$ reactions [3]. The dispersion of the masses found by different experiments remains generally less than 20 MeV. However the widths of these resonances, as reported by the various authors, differ by a large amount. For example, the width of the $N(1440)P_{11}$ resonance, extracted from the $\pi N \to \pi N$ reaction, varies between a lower limit of 135 ± 10 MeV and an upper limit of 545 ± 170 MeV [1]. Moreover, the many theoretical width attributions inside constituent quark models [4] are often much smaller than those reported by the experiments. Such discrepancies between different experimental results and between calculated and experimental widths have sometimes been emphasized, and they have been used for example to test [5] whether the $N(1535)S_{11}$ could be a pentaquark $q^4\bar{q}$ state. It appears therefore that a study of "low-mass" baryon resonances with more precise experiments than those previously performed—with good resolution, small binning, and large statistics—will be a sensitive test for the many existing models. Another important test to select among the models would be to measure, with high precision, the branching ratios for various deexcitation modes. In this respect, a recent theoretical work [6] finds a $B_{N\pi}$ ratio for the $S_{11}(1535)$ varying from $29 \pm 1\%$ to $67 \pm 1\%$ depending on the model considered. This question was also studied in different theoretical papers, with emphasis on positive- and negative-parity resonances [7], or $J^\pi = 3/2^-$ resonances [8].

If we exclude some recent experiments performed at JLab, nearly all previous studies in the nonstrange sector were done without any attempt to have a good resolution and therefore a suitable binning. It is now possible to perform measurements with a better resolution and finer binning than before. Such an experiment was performed at the now-defunct Saturne synchrotron, on the SPES3 beam line.

In this paper the data from the $pp \to ppX$ and $pp \to p\pi^+X$ reactions studied at two incident proton energies, $T_p = 1520$ and 1805 MeV, are reported. The incident energies open up the $\pi^0 p(\pi^+ n)$ and ηp deexcitation channels of the N^* and Δ^+ baryonic resonances. For the first reaction, $pp \to ppX$, mass ranges of $1470 \leqslant M_{pX} \leqslant 1585$ MeV using the lowest incident energy and $1560 \leqslant M_{pX} \leqslant 1680$ MeV using the highest incident energy were studied. The second reaction, $pp \to p\pi^+X$, allows the study of the $n\pi^+$ deexcitation channel of the N^* and Δ^+ baryonic resonances in the range $1470 \leqslant M_{n\pi^+} \leqslant 1640$ MeV and with a slight spectrometer angle dependence.

The study of nucleon resonances is clearly connected with the production of mesons either close to threshold or at higher energies. A great number of papers are related to such studies and not all can be quoted here [9,10].

In the baryonic mass range studied in this paper, one major problem is to distinguish between genuine quark model states and exotic states. Unlike the situation at low baryonic masses, where new narrow states are clearly exotic, for the mass range discussed in this work the answer is not so simple, since, as already stated, the calculated widths of quark model states are sometimes much smaller than the experimental widths reported by the Particle Data Group (PDG). The situation is further complicated by the possibility of connecting new baryons to the "missing resonances" predicted by the constituent quark model but, so far, not observed. Clearly,

*E-mail: tati@ipno.in2p3.fr

measurements of as many properties as possible of the baryonic resonance excitations and disintegrations would be useful.

This paper is constructed in the following way: The main properties of the experimental layout are briefly recalled in the Sec. II. Section III describes the analysis and details the various intermediate results for one given angle and one given missing-mass selection. The different ways of subtracting events giving the experimental signal but corresponding to the "uncorrelated" missing-mass contribution (hereafter called the physical background) will be considered. Results are presented and discussed in Sec. IV, and are compared with many theoretical quark model results. A general discussion then follows and the data for several deexcitation branches are compared. The last section contains a summary of the results and a conclusion.

Our results on narrow baryonic resonances in the mass range $1.0 \leqslant M \leqslant 1.46$ GeV were already published in [11], and those in the mass range $1.72 \leqslant M \leqslant 1.79$ GeV were previously published in [12].

II. PROPERTIES OF THE MAGNET AND DETECTOR LAYOUT

A complete description was already published in a previous paper [11]. This description included a presentation of the experimental setup, the performance of the experimental apparatus, the checks performed, the simulation code used to evaluate raw data normalization, and the various normalizations that had to be introduced. Such a lengthy description will not be repeated here; only the main properties will be given.

The measurements were performed at the Saturne synchrotron beam facility. The experimental signature required the simultaneous detection of two positively charged particles, using the SPES3 spectrometer and detection system. A liquid H_2 target was used. The spectrometer allowed a large momentum range of the detected particles, 600 MeV $< pc <$ 1400 MeV at $B = 3.07$ T, with help of several drift chambers. The trigger consisted of four planes of plastic scintillator hodoscopes. Particles were identified mainly by their time of flight. The particle momenta were determined using one MIT-type and several CERN-type drift chambers. The resolution in the invariant mass spectrum was measured using the final-state interaction peak from the $pp \rightarrow ppX$ reaction. It was close to $\sigma(\Gamma) \approx 0.9$ MeV. The resolution of the missing mass was measured in the neutron missing mass from the $pp \rightarrow p\pi^+X$ reaction at forward angles. It was close to $\sigma(\Gamma) \approx 2.2$ MeV at $\theta = 0.75^\circ$ and $T_p = 1.805$ GeV. At both incident energies, $T_p = 1520$ and 1805 MeV, the data were taken at six angles from $0^\circ(0.75^\circ)$ up to 17° in the laboratory system.

A simulation code was written to check the various properties of the detection system. It reproduces the position and the width of the neutron missing-mass peak [11]. The simulation code is used to obtain the contributions of the peaks, by subtraction of the physical smooth, uncorrelated invariant masses (see Sec. III B).

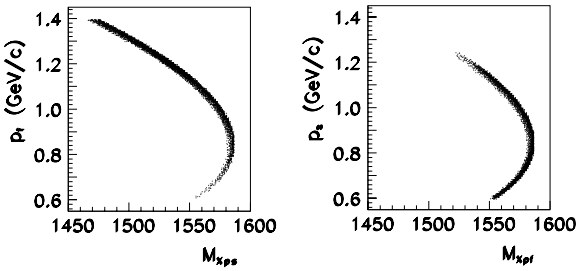

FIG. 1. $pp \rightarrow ppX$ reaction at $T_p = 1520$ MeV and $\theta = 2^\circ$. Scatter plots of fast proton momenta p_f versus the invariant mass M_{Xps} and slow proton momenta p_s versus M_{Xpf}.

III. DESCRIPTION OF THE ANALYSIS

In the $pp \rightarrow ppX$ reaction, each invariant mass M_{pX} studied has two different kinematical solutions, corresponding to different transferred momenta. Figure 1 exhibits the scatter plots of M_{Xp_i} versus p_j $(i \neq j)$ at $T_p = 1520$ MeV, and $\theta = 2^\circ$, where i and j denote the fast (f) and slow (s) detected protons. We see clear cuts, created either by physics or by the momenta limits of the spectrometer: $0.6 \leqslant pc \leqslant 1.4$ GeV. The data must be studied separately for the two branches; otherwise an artificial peak structure will appear in the case of a simple addition. All preliminary spectra, versus M_{p_fX} or M_{p_sX}, will therefore be presented as belonging to either the "upper branch" or "lower branch," depending on whether they are above, or below, the turnback limit in the scatter plots. Here, M_{p_fX} or M_{p_sX} are the invariant masses obtained by using the momenta p_f and p_s of the fast and slow emitted protons, respectively. The two branches were separated through software cuts on the momentum of the proton not included in the invariant-mass (see Fig. 1). These cuts create narrow invariant-mass regions with incomplete efficiencies. These narrow ranges are therefore omitted in the spectra. In a few cases, the sum of the spectra from both branches is performed; the eliminated range resulting from incomplete efficiency is delimited by vertical lines. The missing masses vary from 0 to 600 MeV at forward angles and for the lowest incident energy. Such a range of results opens up the study of the deexcitation of the baryonic resonances into $N\pi^0$ and $N\eta$ channels at forward angles. This range does not allow the study of the disintegration into heavier and still narrower mesons (and nucleons). For increasing spectrometer angles, the resolution diminishes whereas the maximum missing mass decreases. The first effect results from the two terms $\partial M_X/\partial\theta_3$ and $\partial M_X/\partial\theta_4$, where θ_3 and θ_4 are the laboratory angles of both detected protons. At a given angle, the resolution improves for increasing missing mass; this property is due to the term $dM_X = A/M_X$.

At $T_p = 1520$ MeV, the η is no longer observable for angles above 9°. At this incident energy, the $N\pi^0$ deexcitation channel is observable at all six angles studied.

At $T_p = 1805$ MeV, the missing mass varies from 300 to 750 MeV at forward angles, and it varies from 0 to 500 MeV at $\theta = 17^\circ$. Therefore only the $N\eta$ deexcitation channel is studied at forward angles, and $N\pi^0$ is studied at backward angles.

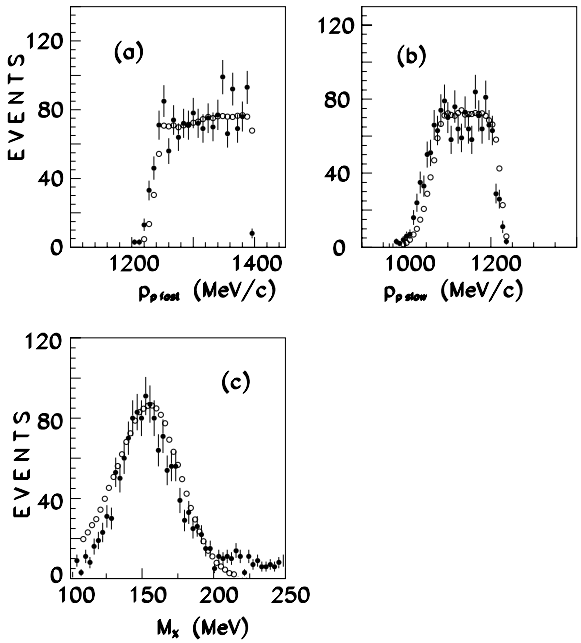

FIG. 2. $pp \to pp\pi^0$ reaction at $T_p = 1520$ MeV, and $\theta = 5^\circ$. Shown are the number of events versus the momenta of the (a) fast and (b) slow proton, for the upper branch of $M_{\pi^0 ps}(M_{\pi^0 pf})$. The lower branches are empty because of the $M_X \leqslant 250$ MeV software cut. (c) The missing mass under the same conditions as in (a). Full points are data and empty points are simulated.

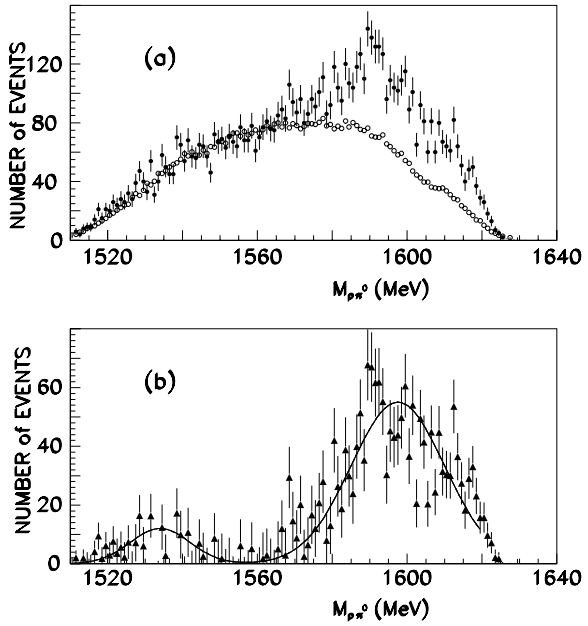

FIG. 3. (a) The number of events of the upper branch of the $M_{\pi^0 ps}$ invariant mass from the $pp \to pp\pi^0$ reaction at $T_p = 1805$ MeV and $\theta = 17^\circ$. Full points are the measured data; empty points are the corresponding normalized simulated events (see text). (b) The difference between data and simulation, representing correlated invariant masses from narrow baryonic resonances.

The $N\pi^0$ ($N\eta$) deexcitation channel is selected through the following software cuts: $M_X \leqslant 250$ MeV($540 \leqslant M_X \leqslant 565$ MeV). The range of the invariant masses differs at both incident proton energies: 1470 MeV $\leqslant M \leqslant$ 1585 MeV at $T_p = 1520$ MeV and $1560 \leqslant M \leqslant 1680$ MeV at $T_p = 1805$ MeV. Since these invariant masses are different, the data will be presented and discussed separately in four different subsections.

A. Comparison of momenta and missing masses with simulations

The simulation code was written in the following way: The events were generated using a flat random distribution of fast-proton momenta and of angular distributions θ_{pf}, θ_{ps}, ϕ_{pf}, and ϕ_{ps}. For angles other than forward ones, a variable distribution of θ_{pf} was introduced between the maximum and minimum possible angles. A Gaussian distribution was introduced for the η width. We take into account the width of the incident beam, the spectrometer resolution, and the detection resolution. We do not introduce the description (mass and width) of any baryonic resonance in the invariant $M_{p\pi}$ mass, nor do we introduce a specific disintegration channel for this resonance. Our simulation therefore describes the shape of uncorrelated events. We expect to observe correlated $p\pi^0$ and correlated $p\eta$ events if these give rise to narrow structures in our invariant mass range. We do not expect to be able to observe the broad PDG baryonic resonances since our mass range is too limited for that and the resonances are mixed. In our relatively small invariant mass range the simulated spectra must be continuous with a slowly varying slope. The measured spectra can display discontinuous shapes, since all reactions studied are exclusive.

A comparison of detected and simulated proton momenta when the missing mass is selected by software cuts to the π^0 is shown in Fig. 2. Figures 2(a) and 2(b) show the momenta distributions of the upper branches of $M_{\pi^0 pf}$ and $M_{\pi^0 ps}$. Full points are data and empty points are the simulation results for $T_p = 1520$ MeV and $\theta = 2^\circ$. Both lower branches are empty. Figure 2(c) shows the missing mass obtained under the same conditions as in Fig. 2(a).

We observe the same global shape for data and simulation, at all angles, for the three variables shown in Fig. 2. This shape is smooth for simulated events and quite dispersed, with non-negligeable error bars, for data.

B. Subtraction of the simulated uncorrelated events

This subtraction is illustrated in detail for the upper branch of $M_{\pi^0 ps}$ at $T_p = 1805$ MeV and $\theta = 17^\circ$. Figure 3(a) shows the data (full points) and the corresponding normalized simulated spectrum (empty points). Over the first half of the range, both distributions nearly coincide; in the second half we observe many more measured events than simulated events. The subtraction between the data and simulated events is shown in Fig. 3(b). These events correspond to correlated $p\pi^0$ from narrow N^* or Δ^+. These results will be discussed in the forthcoming Sec. IV C2.

Another illustration is shown in Fig. 4 for the baryonic resonance deexcitation into the ηn channel with $T_p = 1520$ MeV

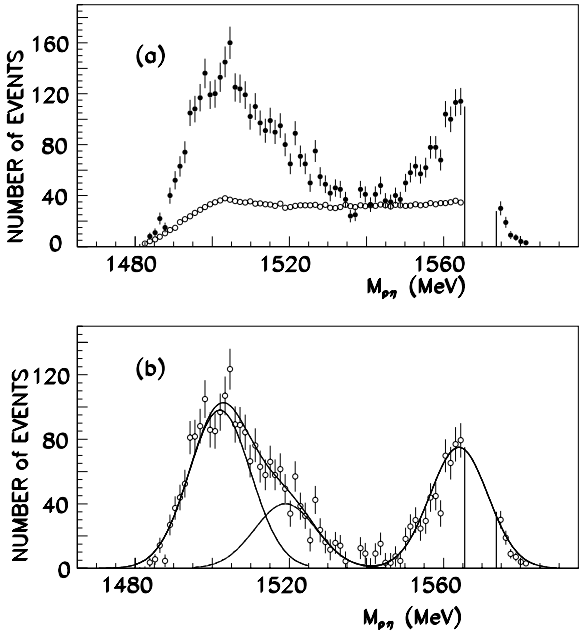

FIG. 4. $pp \to p_f p_s \eta$ scattering at $T_p = 1520$ MeV and $\theta = 2^\circ$. The number of events versus $M_{ps\eta}$ was selected by a cut on p_f to retain only the upper branch events. In (a), the full points are the data and the empty points are the normalized simulated background. In (b), the difference between data and background is presented and is fitted by three Gaussians (see Table I).

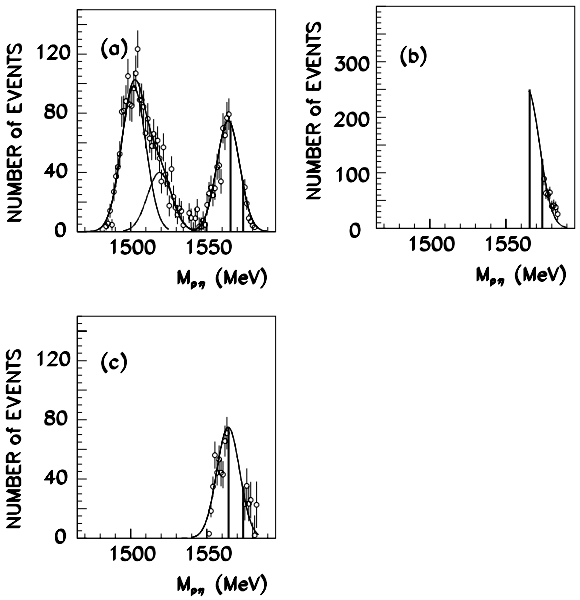

FIG. 5. Data minus normalized simulations for the uncorrelated events at $T_p = 1520$ MeV and $\theta = 2^\circ$. Shown are the number of events versus (a) M_{Xps} when $p_f \geqslant p_f$ limit (upper branch), (b) M_{Xpf} when $p_s \geqslant p_s$ limit (upper branch), and (c) M_{Xpf} when $p_s \leqslant p_s$ limit (lower branch).

and $\theta = 2^\circ$. We observe, from Fig. 1, that the main statistics will appear from the upper branch of M_{Xps}, whereas the corresponding lower branch will give rise to only a few events (and will therefore be omitted). Figure 4(a) shows the data (full circles) and the background from simulation below the $p\eta$ peaks (empty circles). This last spectrum is used for the uncorrelated event description (background). It is normalized to the maximum possible number of events, but the points raised in this paper would not be modified with a smaller selection of uncorrelated events for the background choice. In Fig. 4(b) the difference between the data and the simulated uncorrelated events is shown; it is decomposed into three Gaussians, each having the same width (see Table I).

Figure 5 shows, for three different kinematical conditions, the data minus the normalized simulations for the uncorrelated events, at $T_p = 1520$ MeV and $\theta = 2^\circ$. Figures 5(a)–5(c) exhibit, respectively, the number of events versus M_{Xps} when $p_f \geqslant p_f$limit, versus M_{Xpf} when $p_s \geqslant p_s$limit, and versus M_{Xpf} when $p_s \leqslant p_s$limit. Here again, $p$limit is the momentum value of the turnback in the scatter plot of M_{Xpi} versus p_j, where $j \neq i$. Both Figs. 1 and 5 use the same data, but in the latter the $N\eta$ disintegration channel is selected through software cuts. The reduction in the invariant mass range is particularly important for Fig. 5(b). When applying the same selection at other angles, namely when we observe M_{Xpf} with p_s larger than $p_s$limit and select the $N\eta$ disintegration channel, we obtain a small increase in the statistics for increasing angles up to 9°, followed by a decrease. Given the weak statistics, this last selection of events will not be presented for this disintegration channel at this incident proton energy.

Table II shows that the same mass values and nearly the same widths are obtained from a Gaussian fit of the data in Fig. 5(c). The range of Fig. 5(b) is too small to allow a peak to be extracted; the values extracted from Figs. 5(a) and 5(c) are consistent with the few existing data points.

TABLE I. $pp \to pp\eta$ reaction. Listed are properties (in MeV) of the peaks extracted using different backgrounds at $T_p = 1520$ MeV and $\theta = 2^\circ$. Condition (a) corresponds to the result of the subtraction of the simulated background; condition (b) corresponds to the subtraction of the experimental background in both parts of the η meson window in the missing range (see text). R indicates the ratio of the peak surface relative to the surface of the 1564-MeV peak.

	First peak			Second peak			Third peak		
Condition	Mass	$\sigma(\Gamma)$	R	Mass	$\sigma(\Gamma)$	R	Mass	$\sigma(\Gamma)$	R
(a)	1502	8	1.36	1519	8	0.57	1564	7.5	1
(b)	1502	8	1.43	1519	8	0.71	1563	7.5	1

TABLE II. The $pp \to pp\eta$ reaction at $T_p = 1520$ MeV and $\theta = 2^\circ$. Listed are properties (in MeV) of the peaks extracted in different kinematical conditions. The software cuts select the η meson missing-mass region. (a), (b), and (c) correspond to the result of the subtraction of the simulated background for different kinematical conditions (see text).

Condition	First peak	Second peak	Third peak
(a)	$M = 1502$	$M = 1519$	$M = 1564$
	$\sigma(\Gamma) = 8$	$\sigma(\Gamma) = 8$	$\sigma(\Gamma) = 7.5$
(b)			consistent with
			$M = 1564$
			$\sigma(\Gamma) = 8$
(c)			$M = 1564$
			$\sigma(\Gamma) = 7.5$

C. Subtraction of physical uncorrelated events and background processes

The "background" is constructed by a normalized addition of the total invariant $M_{p\eta}$ mass in both parts, below and above the η meson mass in the missing-mass spectrum. The software cuts chosen are $500 \leqslant M_X \leqslant 525$ MeV and $575 \leqslant M_X \leqslant 600$ MeV, respectively, for both ranges. Figure 6(a) shows the data points with the normalized "background" discussed before, whereas Fig. 6(b) shows the subtracted spectrum, with three Gaussian fits, as before. In Table I, the last line shows the properties of the extracted peaks, which all have the same mass and the same width as before when the simulated "background" is used. The relative surface of the peaks, obtained with help of both backgrounds, moves a little but has no influence on the discussion that will be presented later.

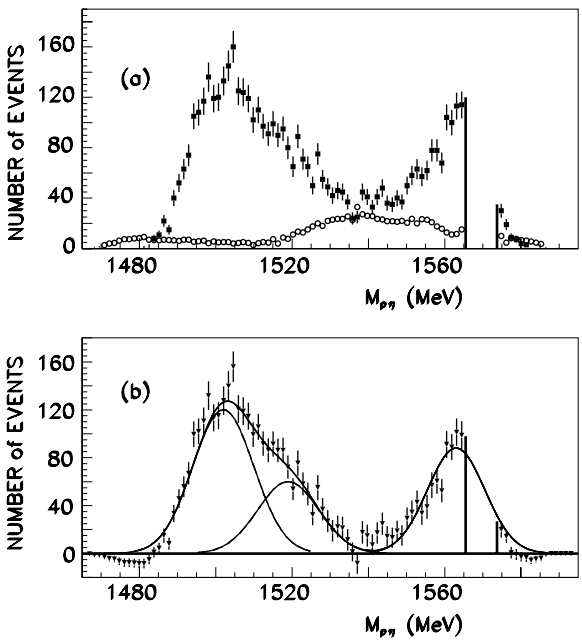

FIG. 6. Same as Fig. 7, except that the normalized background is the physical background obtained by selecting lower and upper parts of the missing mass spectrum around the η meson mass.

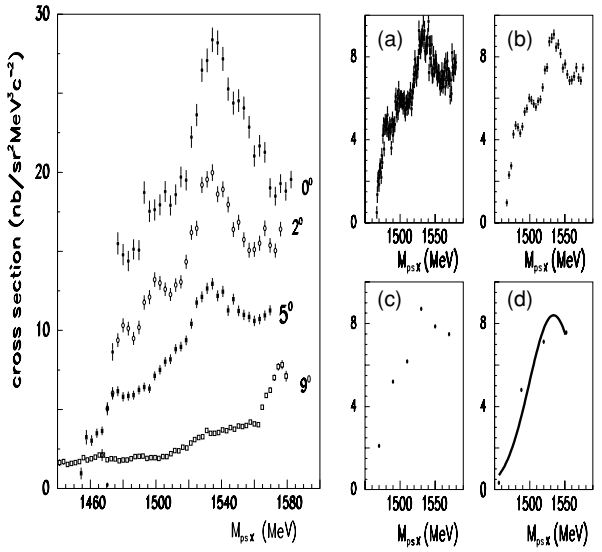

FIG. 7. Upper branch of the $pp \to ppX$ cross sections at $T_p = 1520$ MeV versus M_{psX}. To appear clearly in the same figure the data in (a) are normalized by factors 1.7, 2.2, 3.5, and 2.5 for angles 0°, 2°, 5°, and 9° respectively. The right-hand part of the figure shows the $\theta = 2^\circ$ data with different binnings. Panels (a), (b), (c), and (d) correspond, respectively, to the following binnings: 0.8, 3.2, 19.2, and 32 MeV/channel.

Such an agreement between masses and widths, obtained with help of both choices for the background, allows us to keep the simulated background for the other data presented later on. When the physical background is used, the ranges of background selected on either side of the peak are at least 37.5 MeV away from the central peak. This alleviates the need to include an eventual η meson tail if it is present. One direct consequence of this is an irregular shape on the high-mass side of the background spectrum as shown in Fig. 6.

IV. RESULTS AND DISCUSSION

Different final states will be studied successively. First, we look at the final state without any particular deexcitation channel; then we study the two final states with the deexcitation into $p\pi^0$ ($n\pi^+$) and $p\eta$.

A. The N^* or Δ^+ final state

Partial results of the reactions studied were already shown in Ref. [13]. As previously explained, different spectra must be considered that separate upper and lower branches and the invariant masses M_{psX} and M_{pfX} constructed with the slow and fast protons respectively.

1. The $pp \to p_f p_s X$ reaction at $T_p = 1520$ MeV

(a) Cross sections versus M_{psX}. The cross sections of the upper branch of the $pp \to p_f p_s X$ reaction at $T_p = 1520$ MeV versus M_{psX} are shown in Fig. 7. The left-hand part shows the

results at four forward spectrometer angles: $\theta = 0^\circ, 2^\circ, 5^\circ$, and 9°. Clear peaks are observed close to 1500 and 1535 MeV and also, but less clear, close to 1480 MeV (and possibly close to 1575 MeV). The maximum is close to $M = 1535$ MeV, the mass of the first S_{11} baryonic resonance $J^P = 1/2^-$, $T = 1/2$, but here the observed width $\Gamma_t \approx 25$–40 MeV is much smaller than that expected from the PDG, where the mean value is as large as 150 MeV. Indeed, the PDG reports for $N^*(1535)$ a width varying from 57 to 240 ± 80 MeV. Although it is rather difficult to draw a background below the $M = 1535$ MeV peak, we estimate, at $\theta = 0^\circ$ and 2°, that the maximum of this $M \approx 1535$ MeV peak amounts to $\approx$30% of the total excitation at this mass. There is also, at this mass, room for contributions from other PDG baryonic resonances with smaller and larger masses and also contributions from $N\pi$ and $N\pi\pi$ incoherent phase-space contributions. It therefore seems highly improbable that these peaks are purely the PDG broad resonances; rather they are more likely to be simply parts of them. This point will be clarified later. We suggest that the reason the PDG data are so wide is due to the lack of experimental precision in previous experiments.

The right-hand part of Fig. 7 shows the effect of looking at the same data but using different binnings. The binning in Fig. 7(b) (3.2 MeV/channel) is the same as the one used in the left-hand part of Fig. 7. It corresponds to the experimental resolution. The binning in Fig. 7(d) (32 MeV/channel) is close to the one used in $\pi N \to \pi N$ and $\pi N \to \pi\pi N$ reactions [14,15]. A more recent energy-dependent and single-energy partial-wave analysis of πN elastic scattering data [16] presents the results binned in steps close to 20 MeV. The amplitudes of the photoproduction data were also presented with a binning close to 18 MeV [17]. Many other papers were published from year to year by the same group [18], testing the sensitivity of different reactions to the pion-nucleon coupling constant [19] or studying the parameter of the multipole analysis in the region of the first Δ resonance [20] or in the range of the $N(1535)$ and $N(1650)$ resonances [21].

The small range studied in the lower branch of the $pp \to p_f p_s X$ reaction at $T_p = 1520$ MeV versus M_{psX} does not allow a clear observation of narrow structures [22].

(b) Cross sections versus M_{pfX}. The differential cross sections of the upper branch of the $pp \to p_f p_s X$ reaction at $T_p = 1520$ MeV versus M_{pfX}, exhibit several narrow weakly defined structures [22]. The differential cross sections of the lower branch of the $pp \to p_f p_s X$ reaction at $T_p = 1520$ MeV versus M_{pfX} exhibit again a nonmonotonic behavior [22]. In short, the masses of narrow structures observed at $T_p = 1520$ MeV, in the $pp \to p_f p_s X$ reaction, are close to 1480, 1500, 1533, 1550, 1560, 1567, and 1576 MeV. The masses of the narrow structures extracted from the cross sections of the $pp \to p_f p_s X$ reaction at $T_p = 1520$ MeV versus M_{pfX} are not as stable, when studied with respect to M_{psX}. They look like "sliding" spectra. Such a behavior could eventually be the result of interferences among different resonances. An attempt was made to check this assumption and to extract the relative ratio of amplitudes among resonances of the same quantum numbers. The results were not conclusive and will not be presented here. The small structures observed in these spectra versus M_{pfX} are therefore not included in the summary Table VII.

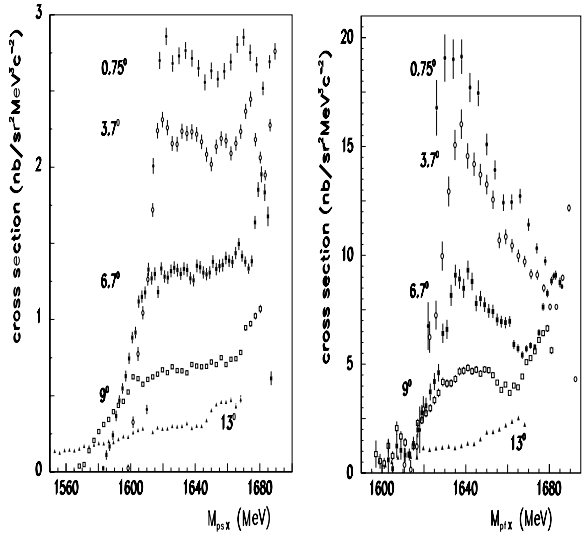

FIG. 8. Cross sections of the upper branch of the $pp \to ppX$ reaction at $T_p = 1805$ MeV. The left-hand part of the figure shows the results from the upper branch versus M_{psX}. To appear clearly in the same figure the data are normalized by factors 3.6, 7.5 10.0, 7.5, and 10.0 for angles 0.75°, 3.7°, 6.7°, 9°, and 13°, respectively. The right-hand part of the figure shows the results from the upper branch versus M_{pfX}. To appear clearly in the same figure the data are normalized by the factors 1, 2.5, 4, 4, and 5 for angles 0.75°, 3.7°, 6.7°, 9°, and 13°, respectively.

2. The $pp \to p_f p_s X$ reaction at $T_p = 1805$ MeV

At this energy, only the upper branch cross sections are shown, since the lower branches, once again, cover a very small invariant mass range ($\Delta M \approx 50$ MeV) and are populated by weak statistics. The left-hand side of Fig. 8 shows the cross sections of the upper part of the $pp \to p_f p_s X$ reaction versus M_{psX}. Narrow peaks are observed close to the following masses (where the question mark means a weaker definition): $M \approx$ (1621?), 1635, and 1668 MeV at $\theta = 0.75^\circ$, $M \approx$ (1620?), 1637, 1669 MeV at $\theta = 3.7^\circ$, $M \approx 1667$ MeV at $\theta = 6.7^\circ$, $M \approx 1600$ MeV at $\theta = 9^\circ$, and $M \approx 1657$ MeV at $\theta = 13^\circ$. However, the last few peaks are small and will therefore be omitted later on in Table VII.

The right-hand side of Fig. 8 shows the cross sections of the upper part of the $pp \to p_f p_s X$ reaction versus M_{pfX}. A main maximum is observed in the four smallest angles at a mass close to $M \approx 1638$–1640 MeV. A small peak is observed close to $M \approx 1660$ MeV in the $\theta = 0.75^\circ$ and 6.7° data.

In summary, the masses of narrow structures observed at $T_p = 1805$ MeV, in the $pp \to p_f p_s X$ reaction, are close to (1600?), (1621?), 1639, 1657, 1660, and 1668 MeV. We observe again a shift, $\Delta M \approx 35$ MeV, between clear peaks, similar to the observations made at small angles and shown in the left-hand side of Fig. 8. Several broad baryonic resonances are reported by the PDG in this mass range; however, the widths of the narrow observed peaks are much smaller than the widths reported by the PDG.

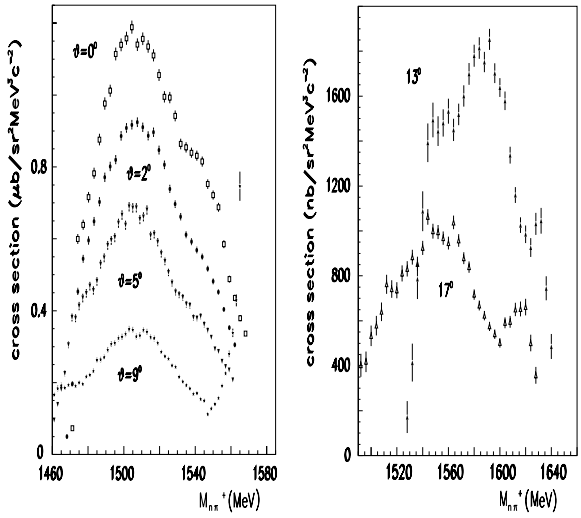

FIG. 9. The left-hand part of the figure shows the differential cross sections of the $pp \rightarrow p\pi^+ n$ reaction versus $M_{\pi^+ n}$, at forward angles and at $T_p = 1520$ MeV. To appear clearly in the same figure, the data, going from top to bottom, are normalized by factors 1.0 at 0° (empty squares), 1.5 at 2° (full circles), 4.4 at 5° (full triangles), and 12 at 9° (empty stars). The right-hand part of the figure shows the same differential cross sections at $T_p = 1805$ MeV, at the two largest measured angles. To appear clearly in the same figure, the data are normalized by factors 1.0 at 13° (full triangles) and 2.0 at 17° (empty triangles).

B. The $n\pi^+$ final state

The reaction $pp \rightarrow p\pi^+ n$ was studied at the same angles and same incident energies as the $pp \rightarrow p_f p_s X$ reaction. The left-hand part of Fig. 9 shows the cross sections versus the four smallest spectrometer angles obtained at $T_p = 1520$ MeV. The maximum, close to $M \approx 1506$ MeV, remains steady at the same mass, regardless of the forward angle of observation, and a shoulder is observed at $M_{n\pi^+} \approx 1540$ MeV. The right-hand part of Fig. 9 shows the cross sections obtained at the two largest angles with maxima close to 1580 and 1540 MeV, respectively, at $\theta = 13^\circ$ and 17°.

C. The $N\pi^0$ deexcitation channel

1. The $N\pi^0$ deexcitation data from baryonic invariant masses obtained with $T_p = 1520$ MeV incident protons

Among the four different kinematical conditions shown in Fig. 1, only two at forward angles contribute to the $M_{p\pi^0}$ missing mass. They are the two upper branches for fast and slow detected protons. The π^0 is not detected in the missing mass for the two lower branches. The results are obtained at the six measured angles: 0°, 2°, 5°, 9°, 13°, and 17°. Narrow structures are extracted at 2° (Fig. 10) and 9° (Fig. 11) [22]. In these figures panels (a) and (b) present the number of events of the upper branches versus M_{Xps} and M_{Xpf}, respectively. Full circles show the data, empty circles show the normalized simulated uncorrelated spectra, considered to be the background, and full triangles show the difference between them. Gaussian peaks are extracted from these last spectra. The quantitative values of these Gaussian fits are reported in Table III. Although the standard deviations found are large, the definition of the peaks depends strongly on the uncorrelated event distributions and are therefore poorly defined. At $\theta = 13^\circ$ (Fig. 12) and $\theta = 17^\circ$ (Fig. 13) three peaks are extracted. The extracted masses of these peaks, at both angles, are about

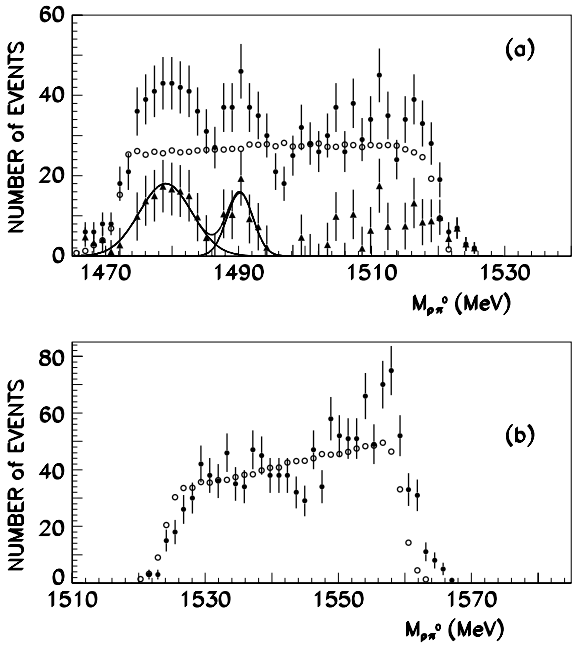

FIG. 10. $pp \rightarrow pp\pi^0$ reaction at $T_p = 1520$ MeV and $\theta = 2^\circ$. Shown are the number of events of the upper branch versus (a) $M_{\pi^0 ps}$ and (b) $M_{\pi^0 pf}$. Full circles show the data and empty circles show the normalized simulated background. Full triangles show the difference between data and simulation. The curves show two Gaussians tentatively extracted from the full triangles spectrum. (See text for more details.)

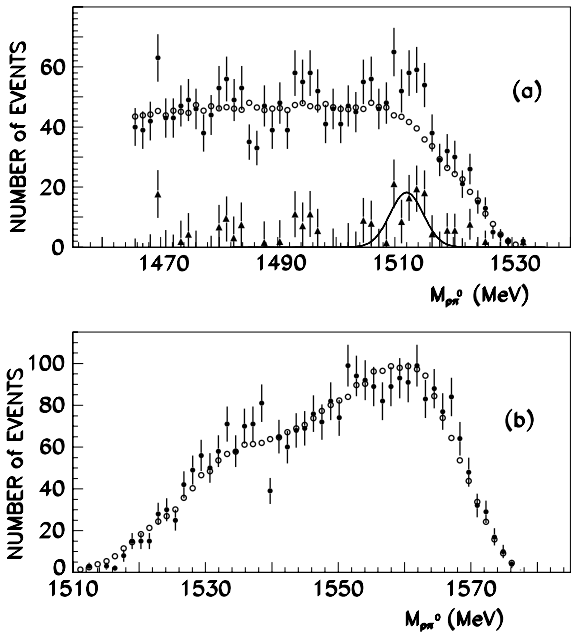

FIG. 11. Same as Fig. 10, but at $\theta = 9^\circ$.

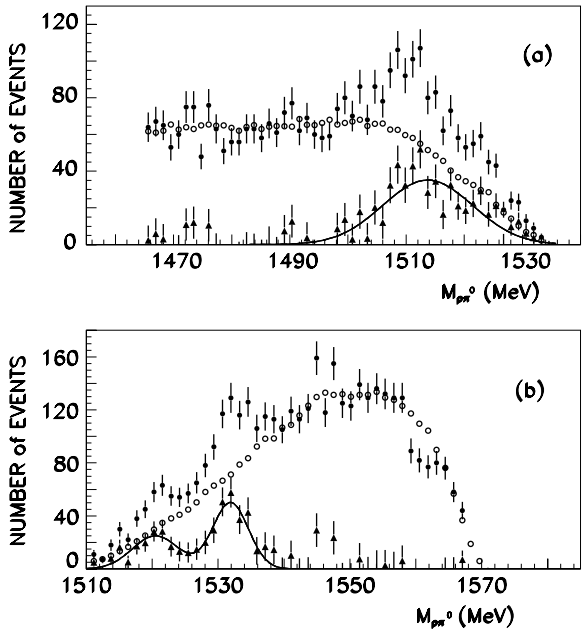

FIG. 12. Same as Fig. 10, but at $\theta = 13^\circ$.

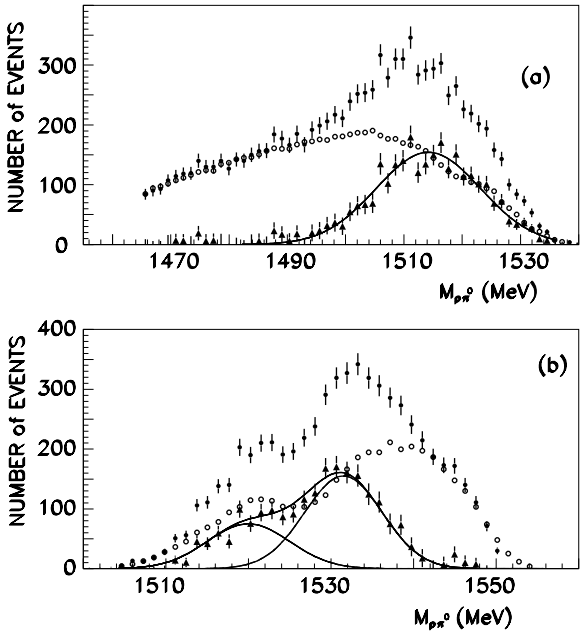

FIG. 13. Same as Fig. 10, but at $\theta = 17^\circ$.

the same (see Table III). These patterns may indicate an oscillatory shape. Table III shows a more or less constant-mass interval between several peaks ($\Delta M \approx 11$ MeV), since the masses of the extracted peaks are close to $M \approx 1479$, 1490, 1513, 1520, and 1532 MeV. In this table R shows the ratio of the peak surfaces (higher mass peak surface divided by lower mass peak surface) where the two peaks are observed under the same kinematical conditions.

At nonforward angles, namely at $\theta = 13^\circ$ and $\theta = 17^\circ$, there are events from the lower branches (see Fig. 1). Figures 14(a) and 14(b) show the number of events versus $M_{\pi^0 pf}$ at $\theta = 13^\circ$, 17° respectively, at $T_p = 1520$ MeV. The statistics are very low when shown as a function of $M_{ps\pi^0}$, and the corresponding data were therefore not studied. In the spectra showing the event population versus $M_{\pi^0 pf}$, two peaks are extracted at the same masses as for the upper branch (Fig. 13), namely at $M \approx 1520$ and 1531 MeV (see Table III).

2. *The $N\pi^0$ deexcitation data from baryonic invariant masses obtained with $T_p = 1805$ MeV incident protons*

The corresponding histograms are empty at forward angles and very few events were accumulated at $\theta = 9^\circ$. The data were studied at the two largest angles: $\theta = 13^\circ$ and $\theta = 17^\circ$. At these angles the number of events is no longer comparable to the forward-angle population since the lower branches are not negligible with respect to the upper branches.

Figure 15 shows the events at $\theta = 13^\circ$ of the upper branch versus $M_{ps\pi^0}$. The data (full points) and simulated events (empty points) are shown in Fig. 15(a) and the difference between the two (full triangles) are shown in Fig. 15(b). There is a hole close to $M_{ps\pi^0} = 1600$ MeV, which arises from

TABLE III. Properties of the peaks extracted at different angles from the $pp \to pp\pi^0$ reaction at $T_p = 1520$ MeV. Panels (a) and (b) show the $M_{\chi ps}$ and $M_{\chi pf}$ data respectively. R denotes the ratio of peak surfaces (higher mass peak divided by the lower mass peak), where the two peaks are extracted under the same kinematical conditions. S.D. is the number of standard deviations of each extracted peak. The masses M and widths $\sigma(\Gamma)$ are in MeV. All figures (except Fig. 14) show upper branch events.

θ (degrees)	Figure	Panel	Branch	Variable	M [$\sigma(\Gamma)$] (MeV)	S.D.	M [$\sigma(\Gamma)$] (MeV)	S.D.	R
2	10	(a)	upper	$M_{\pi^0 ps}$	1479 (3.9)	5.7	1490.2 (2.0)	3.4	0.43
		(b)	upper	$M_{\pi^0 pf}$	—	—	—	—	—
9	11	(a)	upper	$M_{\pi^0 ps}$	1512.0 (2.8)	4.0	—	—	—
		(b)	upper	$M_{\pi^0 pf}$	—	—	—	—	—
13	12	(a)	upper	$M_{\pi^0 ps}$	1513.7 (7.8)	9.1	—	—	—
		(b)	upper	$M_{\pi^0 pf}$	1520.5 (3.5)	6.0	1531.9 (2.7)	8.2	1.54
17	13	(a)	upper	$M_{\pi^0 ps}$	1514.2 (9)	24	—	—	—
		(b)	upper	$M_{\pi^0 pf}$	1520 (5)	12.6	1531.5 (4.7)	21.3	1.94
13	14	(a)	lower	$M_{\pi^0 pf}$	—	—	—	—	—
17		(b)	lower	$M_{\pi^0 pf}$	1520 (5.5)	23.4	1531 (4.7)	15.9	0.55

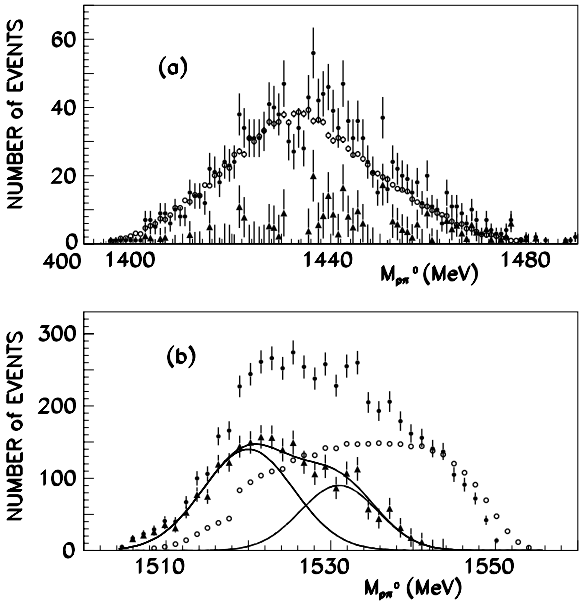

FIG. 14. $pp \to pp\pi^0$ reaction at $T_p = 1520$ MeV and (a) $\theta = 13^\circ$ and (b) $\theta = 17^\circ$. Shown are the number of events of the lower branch versus $M_{pf\pi^0}$. Full circles show the data, empty circles show the normalized simulated background, and full triangles show the difference between measured and simulated data. See text for more details and Table III for quantitative information.

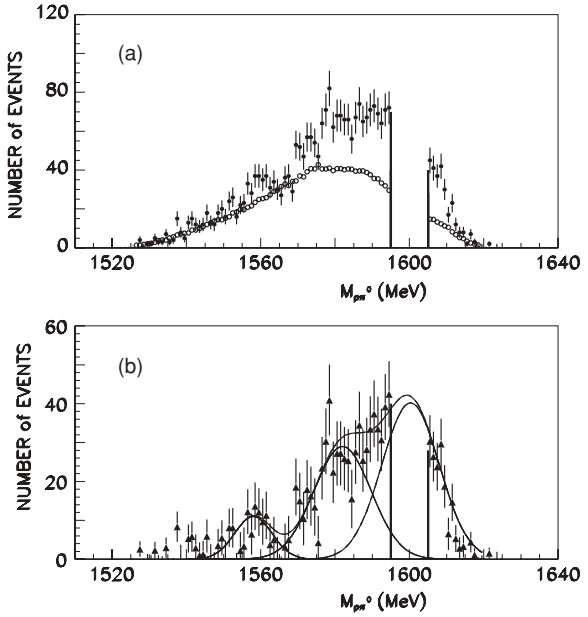

FIG. 15. $pp \to pp\pi^0$ reaction at $T_p = 1805$ MeV and $\theta = 13^\circ$. Shown are the number of events of the upper branch versus $M_{ps\pi^0}$. Panel (a) shows the data (full points) and simulated uncorrelated events (empty points). Panel (b) shows the difference between both (full triangles) and an attempt to extract three Gaussians from the spectrum.

the region where both p_f and p_s detected proton momenta are similar. To avoid such invariant mass ranges with lost events, the following software cuts were applied: All events were suppressed ($M \approx 1600$ MeV), when the difference between both momenta was lower than 50 MeV/c. The mass range $1595 \leqslant M \leqslant 1605$ MeV was therefore removed from Fig. 15. The quantitative information is given in Table IV. Figure 16 shows the corresponding events from the upper branch versus $M_{pf\pi^0}$. Again, there is a hole in the data close to $M_{p\pi^0} = 1611$ MeV, which correponds to the region where both proton momenta are equal. However, the simulated results show that the hole is a real physical effect. The data show two peaks described by two Gaussians centered at masses (widths) $M = 1605.7$ [$\sigma(\Gamma) = 3.4$] MeV and $M = 1622$ [$\sigma(\Gamma) = 5.4$] MeV, rather than a single Gaussian at $M = 1616$ [$\sigma(\Gamma) = 8.7$] MeV. However, because a (small) ambiguity owing to the lost events remains, these results are removed from the general summary and from Tables IV and VII.

A careful detailed analysis was performed at the largest spectrometer angle ($\theta = 17^\circ$). Figures 3 and 17 show the number of events of the upper branches versus the invariant masses $M_{ps\pi^0}$ and $M_{pf\pi^0}$, respectively, at $\theta = 17^\circ$ and $T_p = 1805$ MeV. Figure 18 shows the sum of the data shown in Fig. 3(b) and Fig. 17(b) (i.e., the data minus the simulation of both upper branches). The lower branches contain few events, and Table IV shows that when all upper and lower branches are added (last line of Table IV), the peaks are extracted at the same mass values that were observed before the addition of the lower branches. A check was performed to ascertain that the dip at $M_{p\pi^0} \approx 1607$ MeV was not produced by an instrumental cut or created by a software cut. With this end in view, software cuts were applied to remove the range $1600 \leqslant M_{p\pi^0} \leqslant 1610$ MeV in the upper branch data, and the effect on the scatter plot of p_f versus p_s was studied. We find that with this software cut there is an overall reduction in the statistics over the whole scatter plot. This means that the discussed range is not connected to a particular range of momenta. Therefore, the dip is from a

TABLE IV. Missing mass from the $pp \to p_f\, p_s\pi^0$ reaction at $T_p = 1805$ MeV, $\theta = 13^\circ$ and 17°.

Figure	Insert	θ	Variable	Branch	$M(\sigma(\Gamma))$	$M(\sigma(\Gamma))$
15	(a) and (b)	13	$M_{\pi^0 ps}$	upper	1558 (5) 1600 (7.7)	1582 (7.7)
16	(a) and (b)	13	$M_{\pi^0 pf}$	upper		
3	(a) and (b)	17	$M_{\pi^0 ps}$	upper	1534.0 (8.0)	1597.5 (12.5)
17	(a) and (b)	17	$M_{\pi^0 pf}$	upper	1601.1 (4.0)	1622.6 (7.5)
18		17	$M_{\pi^0 pf}$ and $M_{\pi^0 ps}$	upper and lower	1602 (6.4)	1620.5 (7.9)

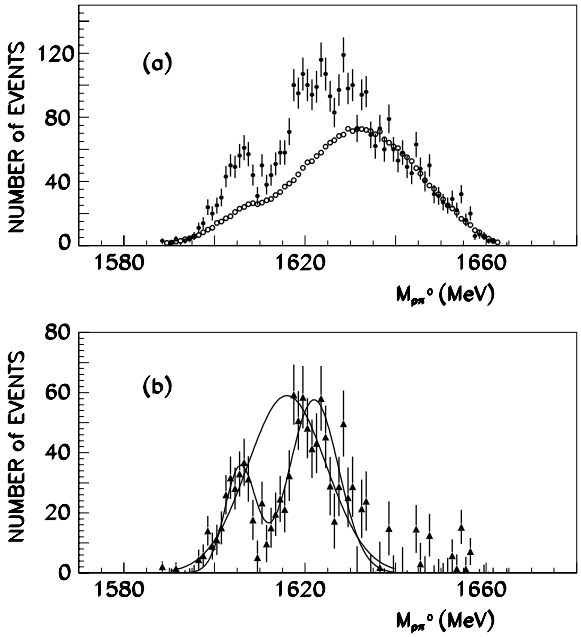

FIG. 16. Same as Fig. 15, but versus $M_{pf\pi^0}$. Two different possible descriptions of the data, with one or two Gaussians, are shown, although the description with two Gaussians is preferred (see text).

physical source as are the two peaks. Quantitative information is given in Table IV.

From these measurements at $T_p = 1805$ MeV, we extracted five peaks close to the following masses: 1534, 1558, 1582, 1601, and 1622 MeV. The three first masses are observed only once, but the last two masses are observed six and four times, respectively. The shift among these five masses is more or less constant: $\Delta M \approx 22$ MeV.

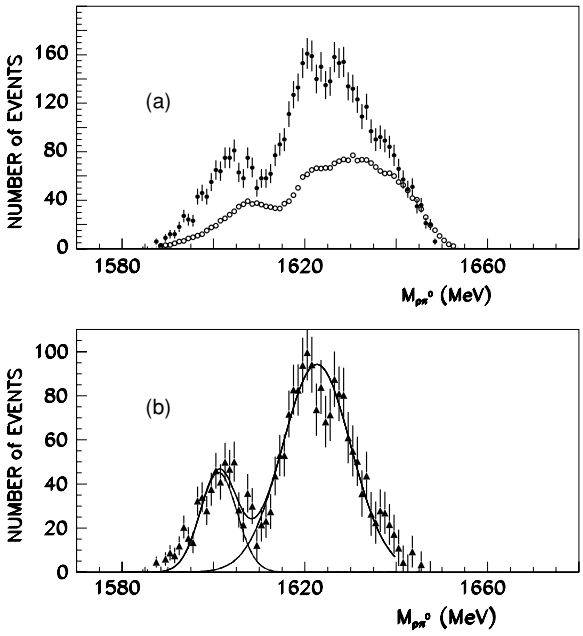

FIG. 17. Same as Fig. 3, but versus $M_{pf\pi^0}$.

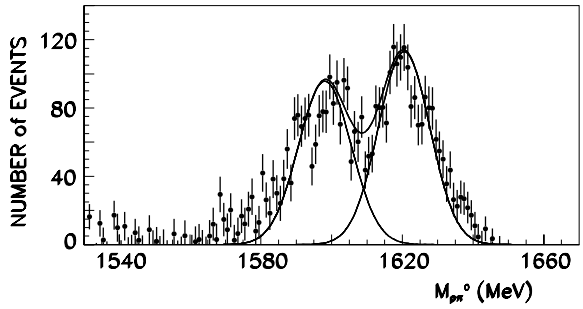

FIG. 18. The $pp \rightarrow pp\pi^0$ reaction at $T_p = 1805$ MeV and $\theta = 17^\circ$. Addition of data from both upper branches. The quantitative information is given in Table IV.

D. The $N\eta$ deexcitation channel

1. The $N\eta$ deexcitation data from baryonic invariant masses obtained with $T_p = 1520$ MeV incident protons

Figure 19 shows the missing mass M_X at $T_p = 1520$ MeV and $\theta = 0^\circ$ for the four kinematical situations. Figures 19(a)–19(d) correspond to the upper part of p_s, the upper part of p_f, the lower part of p_s, and the lower part of p_f, respectively. The η is clearly observed in Figs. 19(b) and 19(c). The data corresponding to the conditions of Figs. 19(a) and 19(d) will not be studied. The η is selected by applying the following software cut: $540 \leqslant M_X \leqslant 565$ MeV.

(a) Study of $p_{pf} \geqslant p_{pf}$ limit data. The results for the smallest angles, where the η meson is observed in our experimental conditions are shown in Figs. 20, 4, 21, and 22 which give plots the number of events of the upper branch of the invariant mass $M_{ps\eta}$ for $\theta = 0^\circ, 2^\circ, 5^\circ$, and 9°, respectively. The values of the extracted peaks are given in Table V. The peak

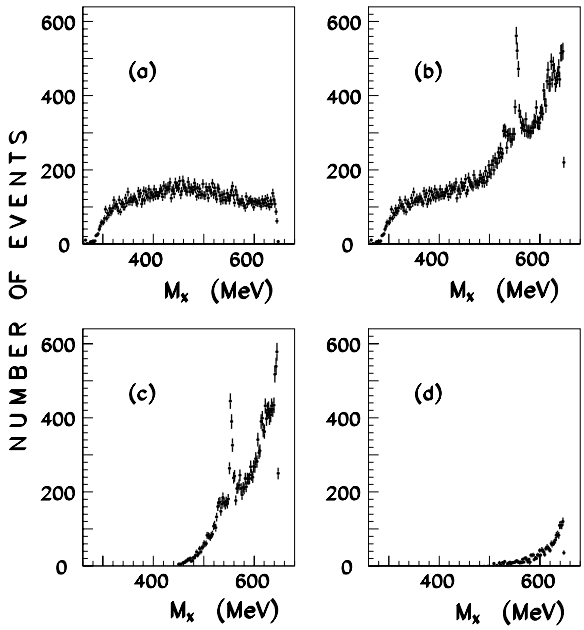

FIG. 19. The $pp \rightarrow ppX$ reaction at $T_p = 1520$ MeV and $\theta = 0^\circ$. Showing the missing mass M_X for (a) $p_s \geqslant p_s$ limit, (b) $p_f \geqslant p_f$ limit, (c) $p_s \leqslant p_s$ limit, and (d) $p_f \leqslant p_f$ limit.

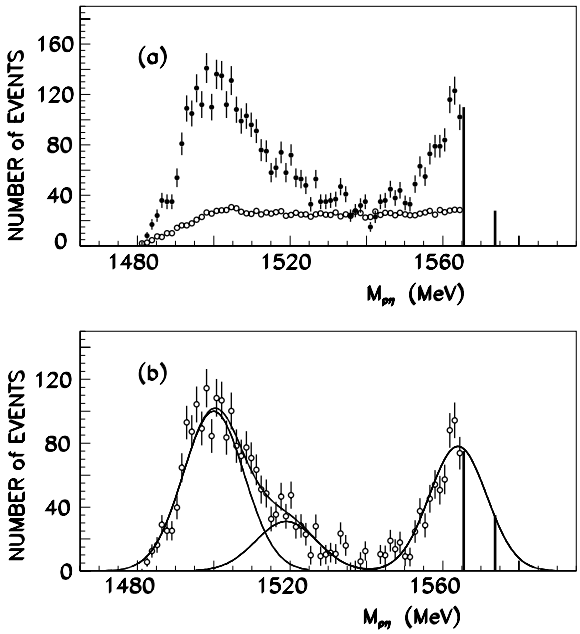

FIG. 20. The $pp \to pp\eta$ data, selected by software cuts, at $T_p = 1520$ MeV and $\theta = 0^\circ$. Panel (a) shows the data of the upper branch (full points) and the corresponding normalized simulated background (empty points) versus $M_{ps\eta}$. Panel (b) shows the data minus the background spectrum, along with the extracted Gaussians.

TABLE V. Missing mass from the $pp \to p_f p_s \eta$ reaction at $T_p = 1520$ MeV. Listed are properties of the peaks extracted at different angles. The software cuts select the η meson missing-mass region. The masses and widths $[\sigma(\Gamma)]$ are in MeV. R denotes the peak surface relative to the peak surface at $M = 1564$ MeV. The masses and widths are in MeV.

Angle	Figure	Branch	Variable	Mass	$\sigma(\Gamma)$	R
0°	20	upper	$M_{ps\eta}$	1500	8	1.37
				1519	8	0.42
				1564	7.5	1
2°	4	upper	$M_{ps\eta}$	1502	8	1.36
				1519	8	0.57
				1564	7.5	1
5°	21	upper	$M_{ps\eta}$	1502	8.5	0.09
				1520.5	9	1.08
				1567	8	1
9°	22	upper	$M_{ps\eta}$	1564.2	6	1
0°	23	lower	$M_{pf\eta}$	1561.5	6.5	1
				1580	6.5	0.68
2°	24	lower	$M_{pf\eta}$	1562.4	6	1
				1580.1	6	1.15
5°	25	lower	$M_{pf\eta}$	1560.1	6.5	1
				1576.2	6.1	1.08
9°	26	lower	$M_{pf\eta}$	1553.1	6.3	0.35
				1567.0	5.3	1

at $M \approx 1564$ MeV is not well defined and is only tentatively extracted at $\theta = 0^\circ$ and 5° by analogy with its behavior at $\theta = 2^\circ$ and 9°, where some points remain on the high-tail side. Three peaks are extracted at $M_{p\eta} \approx 1502$- and 1519- MeV and tentatively at $M_{pz} \approx 1564$ MeV. The R values give the relative angular variation of the surface of the three extracted peaks to the surface of the $M \approx 1564$ MeV peak. They are listed in Table V. They must be considered as being tentative, since the surfaces are somewhat imprecise. We observe an increase of the second ratio with increasing angle. It is not possible to use this result to discuss the relative spins of both states $M \approx 1517$ and 1564 MeV. Indeed, the transferred momenta vary differently for these different final states with increasing angle. The two other ratios are consistent with a constant value.

Three masses are extracted from our spectra: $M \approx 1502$, 1520, and 1565 MeV. The second mass is the same as the one extracted with a software selection to $N\pi^0$. The width here is larger: $\sigma(\Gamma) \approx 8$ MeV instead of $\sigma(\Gamma) \approx 4$ MeV. There is a peak at the same mass reported by the PDG [1], namely the D_{13}, but with a total width $\Gamma \approx 120$ MeV. No peak was extracted at $M \approx 1502$ MeV from the $N\pi^0$ deexcitation data. There is no broad resonance reported at either $M \approx 1502$ MeV or $M \approx 1564$ MeV.

(b) Study of $p_{ps} \leqslant p_{ps}$limit data. Figures 23–26 show the number of events versus the lower branch of $M_{pf\eta}$ for angles $\theta = 0^\circ$, 2°, 5°, and 9°, respectively, at $T_p = 1520$ MeV. For this kinematical configuration, $\theta = 9^\circ$ is again the maximum possible spectrometer angle. The quantitative information is given in Table V. Three peaks are extracted, a peak at $M_{pf\eta} \approx 1553$ MeV, seen only once at $\theta = 9^\circ$ and therefore less well defined than the two others, and two peaks close to $M_{pf\eta} \approx 1562$ and 1579 MeV. The mass of the first of these two peaks is very close to a mass observed previously in different data, namely the upper part of $M_{ps\eta}$, since the mass difference is only $\Delta M \approx 2$ MeV. There is no broad PDG baryon with any of these three masses. The R values in Table V show the relative peak intensities with respect to the $M \approx 1564$ MeV peak. The angular variation of this ratio is flat and may be considered as being consistent with a value of 1.

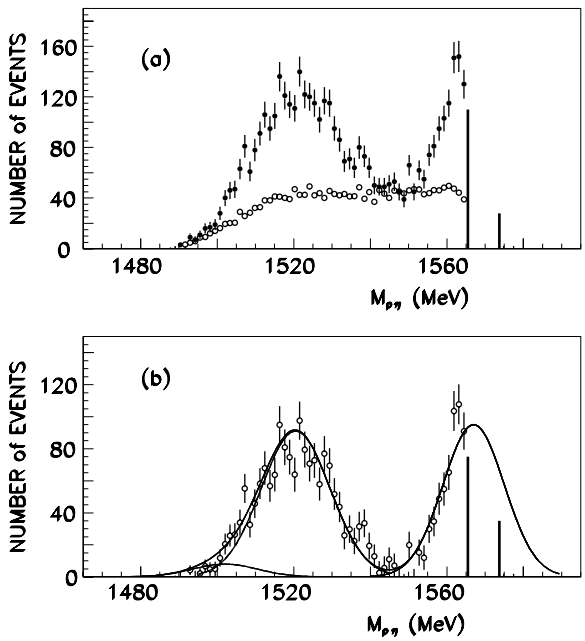

FIG. 21. Same as Fig. 20, but for $\theta = 5^\circ$.

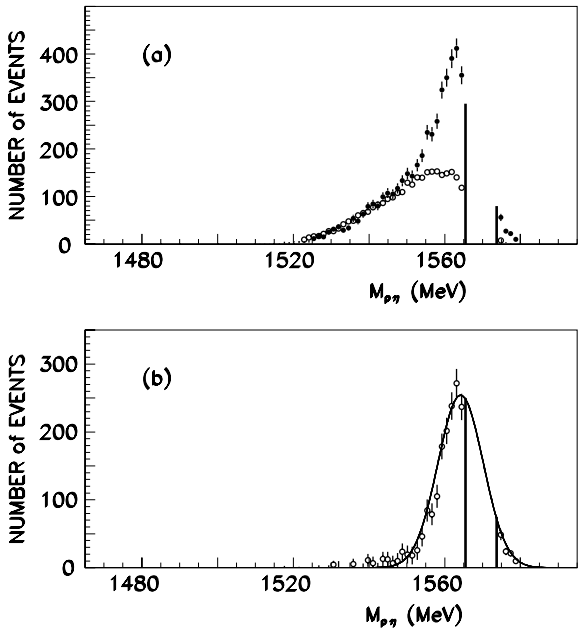

FIG. 22. Same as Fig. 20, but for $\theta = 9^\circ$.

2. *The $N\eta$ deexcitation data from baryonic invariant masses obtained with $T_p = 1805$ MeV incident protons*

In the missing mass at $T_p = 1805$ MeV and $\theta = 0.75^\circ$, clear M_η peaks are observed, superposed on large backgrounds. The statistics of the lower branch are small and no η meson peak is clearly observable in the missing-mass spectra. This is illustrated in Fig. 27. Figure 27(a) shows the addition of both upper branch data, to be compared to Fig. 27(b), which shows the addition of both lower branch data. Data between both vertical lines are removed since they correspond to the transition region between $M_{pf\eta}$ and $M_{ps\eta}$ where some events are lost as the result of the software cuts applied between upper and lower branches. Figure 27(c) shows the total spectrum of all branches.

Figure 27(c) shows a peak superposed on a background. This background corresponds to uncorrelated events and is presented in Fig. 28 with the help of our simulation code. Figure 28(a) shows the renormalized simulated events at $T_p = 1805$ MeV and $\theta = 0.75^0$ from the upper branch of

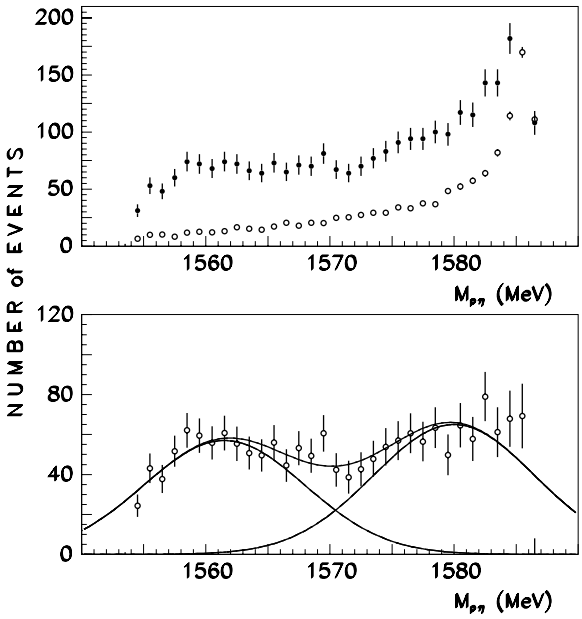

FIG. 23. Number of events of the lower branch of the $pp \to pp\eta$ reaction, selected by software cuts, at $T_p = 1520$ MeV and $\theta = 0^\circ$. The top panel shows the data (full points) and the normalized simulated background (empty points) versus $M_{pf\eta}$. The bottom panel shows the data minus the background, along with the extracted Gaussians.

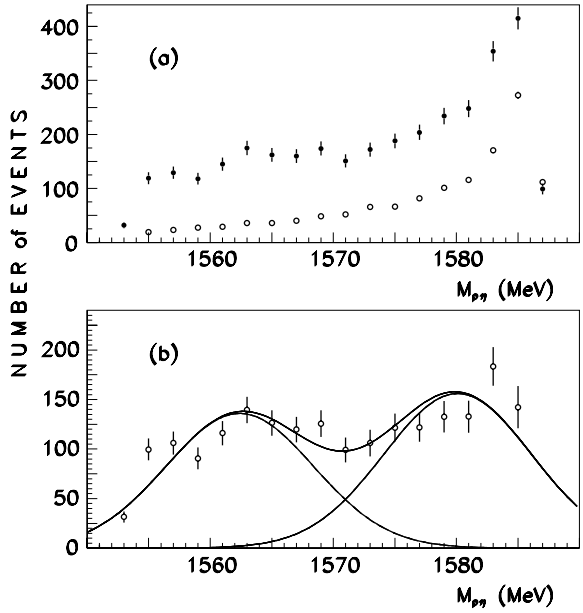

FIG. 24. Same as Fig. 23, but for $\theta = 2^\circ$.

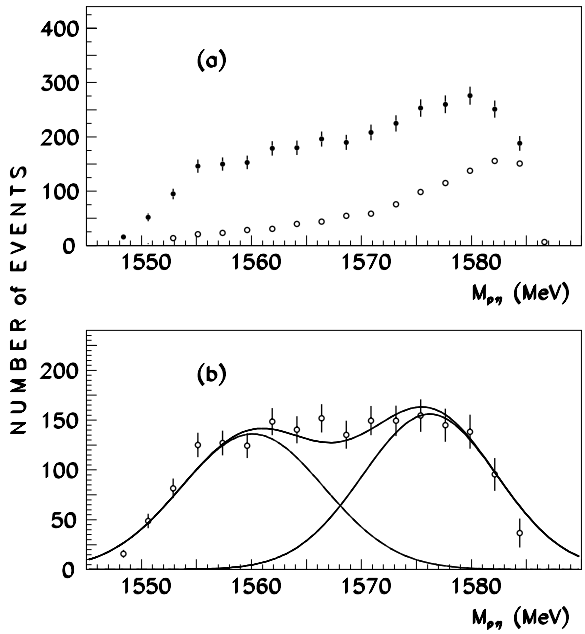

FIG. 25. Same as Fig. 23, but for $\theta = 5^\circ$.

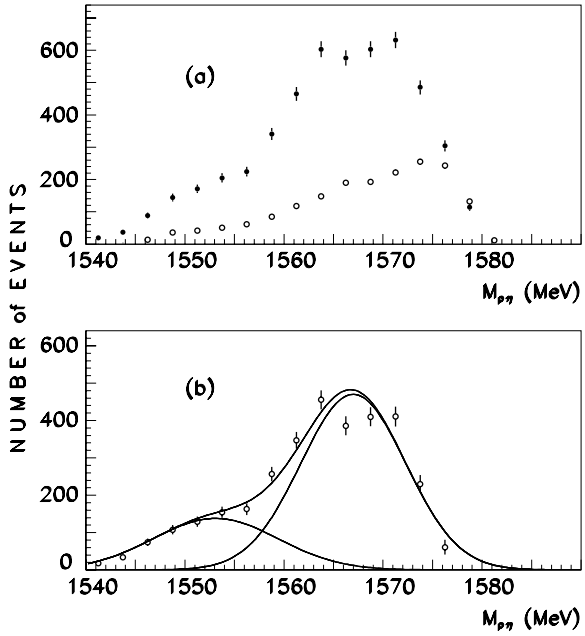

FIG. 26. Same as Fig. 23, but for $\theta = 9^\circ$.

$M_{pf\eta}$ (empty circles) and from the upper branch of $M_{ps\eta}$ (full circles). These simulated data are fitted by two straight lines. Figure 28(b) shows the same results for $\theta = 3.7^\circ$. The normalized lines fitting the "background" are reported in Fig. 27(c).

Figure 29 shows the data for $\theta = 3.7^\circ$ presented in the same way as in Fig. 27 (for $\theta = 0.75^\circ$). The simulation and data for $\theta = 6.7^\circ$ are shown in Figs. 30 and 31.

Figure 32 shows the spectra extracted from the $pp \to p_f p_s \eta$ reaction at $T_p = 1805$ MeV at the three forward angles

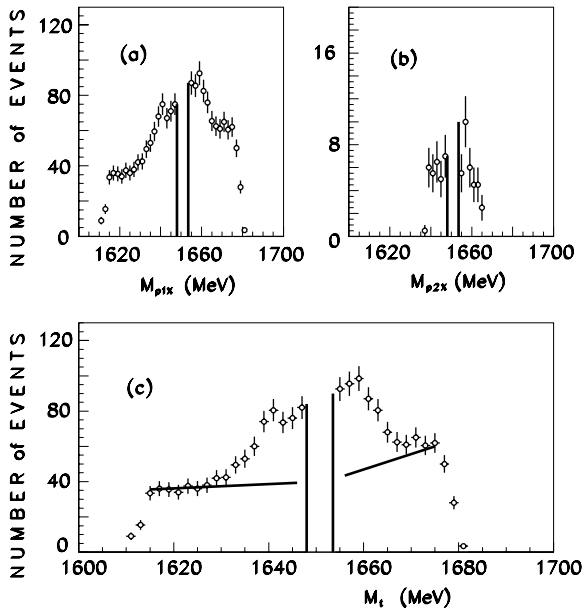

FIG. 27. The $pp \to pp\eta$ reaction at $T_p = 1805$ MeV and $\theta = 0.75^\circ$. Showing (a) data from both upper branches (b) data from both lower branches and (c) data from all four branches. The simulated background is reported by two straight lines.

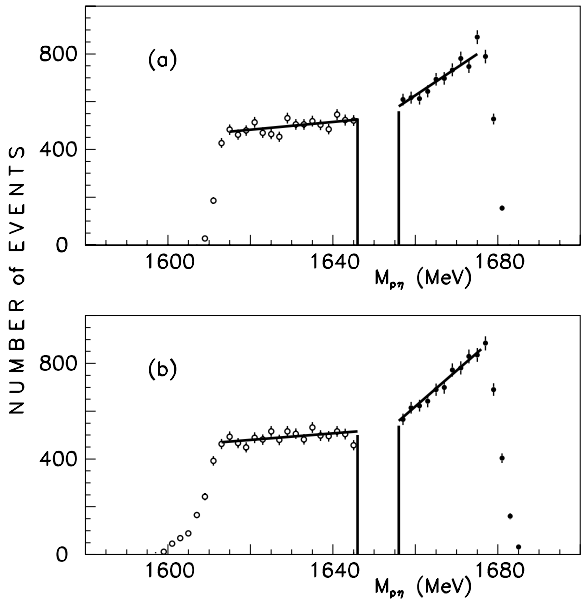

FIG. 28. The $pp \to pp\eta$ reaction at T_p=1805 MeV, showing the simulated events at (a) θ=0.75°, and (b) $\theta = 3.7^\circ$ from the upper branch of $M_{pf\eta}$ (empty symbols) and from the upper branch of $M_{ps\eta}$ (filled symbols). This simulated data are fitted by two straight lines.

$\theta = 0.75^\circ, 3.7^\circ$, and 6.7°. These data came from the subtraction of total events minus uncorrelated simulated events shown in Figs. 27, 29, and 31 for angles $\theta = 0.75^\circ, 3.7^\circ$, and 6.7°, respectively. Two peaks at $M \approx 1642$ and 1658.5 MeV are extracted at all three angles. The quantitative information is given in Table VI. The ratio R, shown in Fig. 33, gives the angular distribution of the relative excitation between the $M \approx 1642$ MeV and the $M \approx 1658.5$ MeV peaks. The error bars are arbitrarily set at $\delta R/R = 0.15$. As previously explained, the different transferred momenta variation, as a function of the angle, prevents drawing any conclusion on the different spins of these two states.

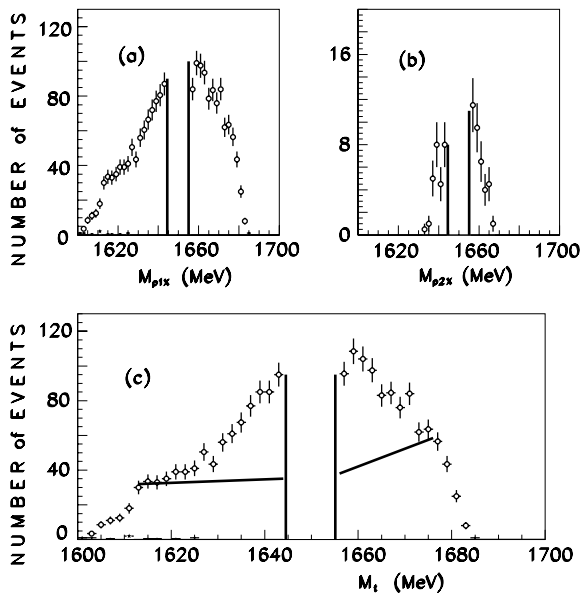

FIG. 29. Same as Fig. 27, but for $\theta = 3.7^\circ$.

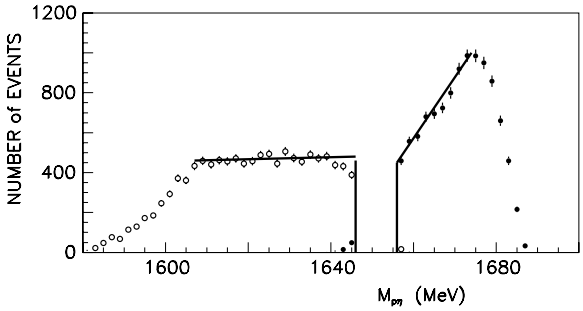

FIG. 30. Same as Fig. 28, but for $\theta = 6.7^\circ$.

Although the missing mass range is not larger than 70 MeV, the observed shape is not the consequence of a low acceptance resulting from cuts applied at both edges of the range. These cuts can be clearly seen on both sides of the spectra in Figs. 27(c), 29(c), and 31(c) and affect four or five channels only on each side.

V. GENERAL DISCUSSION OR COMPARISON BETWEEN BOTH DEEXCITATION BRANCHES

Several N^* and Δ baryons are reported in [1] to exist in the mass range $1440 \leqslant M \leqslant 1700$ MeV. They all appear with four stars in the $N\pi$ deexcitation mode. Two baryonic resonances are reported to have four stars in the $N\eta$ desexcitation mode: the $N(1535)$ and $N(1650)$, both S_{11}. In this channel the observed structures cannot come from any Δ resonance.

All our structures have smaller widths than those reported in [1] for the baryonic resonances. They are also weakly excited compared to the excitation of the PDG resonances. It is therefore tempting to associate our narrow structures to the PDG broad ones, providing the latter have a "fine structure."

By analogy with the nuclear giant resonances, we can argue that the baryonic resonances are so broad that their lifetime

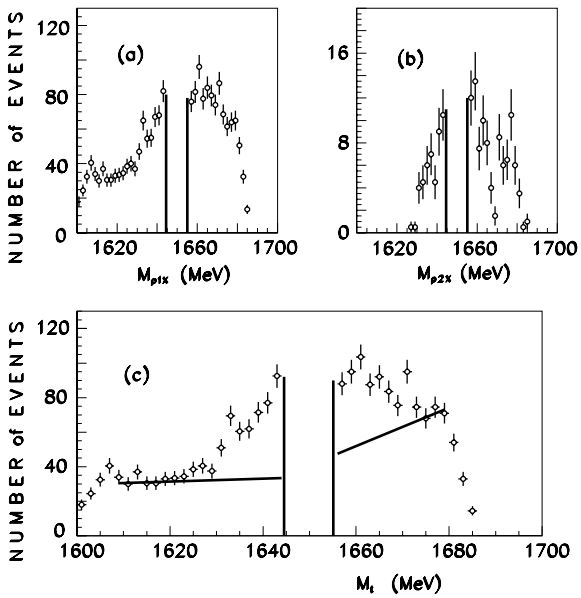

FIG. 31. Same as Fig. 29, but for $\theta = 6.7^\circ$.

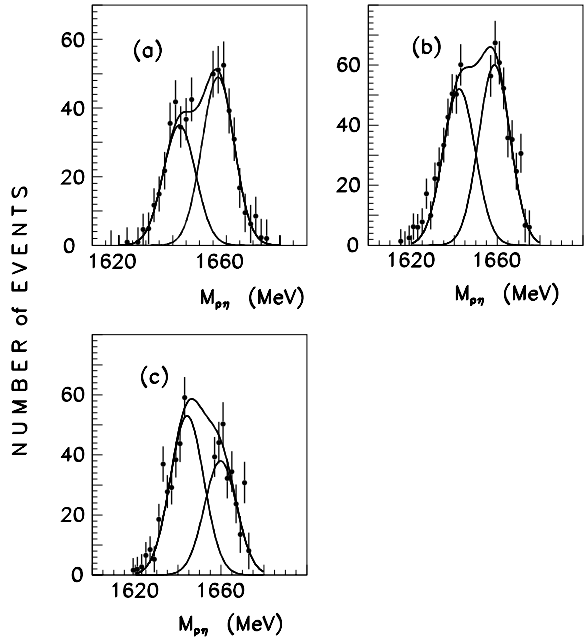

FIG. 32. The $pp \to pp\eta$ reaction at $T_p = 1805$ MeV and (a) $\theta = 0.75^\circ$, (b) $\theta = 3.7^\circ$, and (c) $\theta = 6.7^\circ$. The points show the total data minus the normalized uncorrelated background simulated data.

is smaller than 10^{-23} s. Their deexcitation takes place very quickly, without time for internal reorganizations. Therefore information on their microscopic structure is conserved. The narrow observed peaks may be signatures of these internal structures.

We observe that interferences between two broad classical baryonic resonances never produce peaks in the middle region between them, but they do produce shifts, usually by ± 10 (± 20) MeV of the maximum of the considered resonance. Therefore, the many narrow observed peaks cannot result from interferences.

Table VII shows the quantitative information for the narrow peaks extracted. Some peaks, being too poorly defined, are omitted. The overall data are plotted in Fig. 34, where the channel is defined in Table VII. The dashed areas show the range of study allowed by the physics and the spectrometer momenta acceptance. All broad baryonic PDG resonances

TABLE VI. Missing mass from the $pp \to p_f p_s \eta$ reaction at $T_p = 1805$ MeV. Listed are properties of the peaks extracted at different angles. The software cuts select the η meson missing-mass region. The masses and widths [$\sigma(\Gamma)$] are in MeV. R gives the ratio of the first peak relative to the second peak.

Angle	Mass	$\sigma(\Gamma)$	R
0.75°	1642.5	6	0.71
	1656.9	6	
3.7°	1642.3	7.5	0.89
	1658.7	7.3	
6.7°	1644.2	7.8	1.45
	1659.8	7.5	

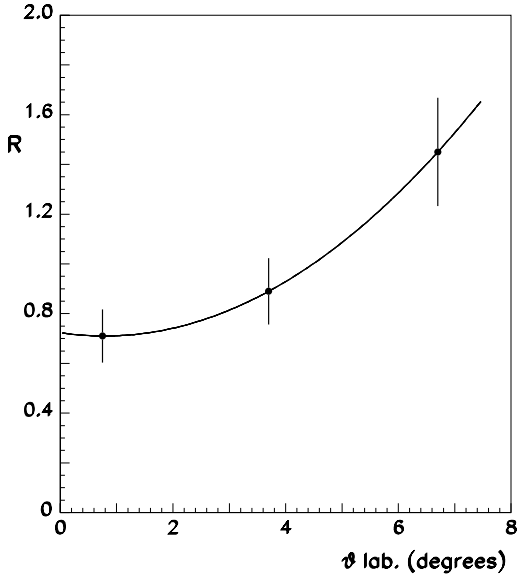

FIG. 33. The $pp \to pp\eta$ reaction at $T_p = 1805$ MeV. The ratio R shows the relative excitation between the $M \approx 1639$ MeV and the $M \approx 1659$ MeV peaks at three forward angles, where both peaks were extracted.

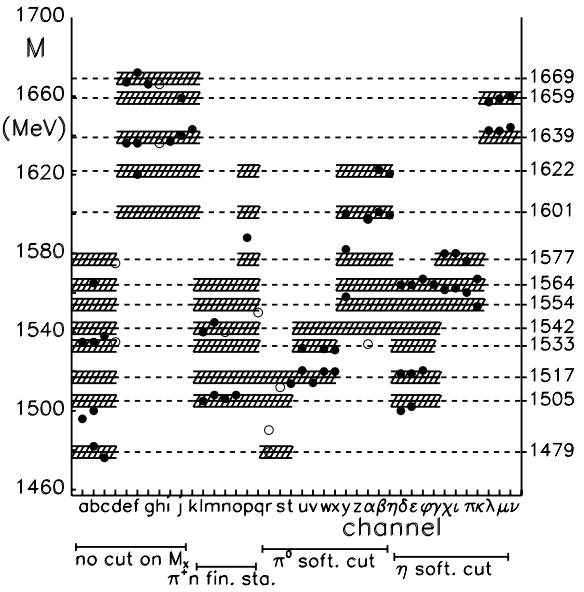

FIG. 34. Masses (in MeV) of the narrow structures extracted from $pp \to ppX$ and $pp \to p\pi^+ n$ reactions in the mass range $1470 \leqslant M \leqslant 1680$ MeV. Full (empty) circles correspond to well-defined (less well defined) peaks. Each column corresponds to a particular experimental situation [reaction, incident energy, angle, upper or lower branch, and invariant mass reconstructed using the slow (fast) proton]. The mass ranges studied differ with different reactions; they are indicated by a dashed area. The mass values of these areas are defined in the following way: The mean value of several masses of narrow peaks is kept as being a narrow peak mass, and the area is drawn with ± 3 MeV range. The quantitative information is given in Table VII.

have an important $N\pi$ deexcitation channel. We make the assumption that the same is true for the narrow baryonic resonances, even if the spectrometer limits prevent their detection. We observe in Fig. 34 that the many masses of narrow peaks $M \pm \Delta M$, where $\Delta M = 3$ MeV, can be brought together into 13 masses shown in the right-hand part of the figure. The full (empty) circles indicate the welldefined (less welldefined) peaks.

The mean values of the extracted masses are close to 1479, 1505, 1517, 1533, 1542, 1554, 1564, 1577, 1601, 1622, 1639, 1659, and 1669 MeV. Most observations have been made several times at the same mass, as can be seen in Fig. 34. However, they have different disintegration modes. As previously discussed, the $pp \to pp\pi^0$ and $pp \to p\pi^+ n$ reactions are different from the dynamical point of view since in the first one the π^0 is not detected and has a small momentum, whereas in the second reaction the π^+ is detected and therefore has a higher momentum ($p_{\pi^+} \geqslant 600$ MeV/c).

Some masses are seen in both $N\pi$ and $N\eta$ channels others are seen in the $N\pi$ channel and not in the $N\eta$ channel. One mass, $M = 1564$ MeV, is seen in the $N\eta$ channel and is not seen in the $N\pi$ channel, although the experimental acceptance allows such an observation. Figure 35 shows the same results. The left-hand part shows the masses disintegrating through the $N\eta$ channel, and the right-hand part shows the masses disintegrating through the $N\pi$ channel. The broad dark lines correspond to broad PDG resonances. The vertical lines are dashed when the disintegration mode is not observed but is likely to exist.

A. Masses disintegrating into $N\pi$ and $N\eta$

Two groups of masses disintegrate through $N\pi$ and $N\eta$ modes. The first one corresponds to the following masses: 1505, 1517, 1554, 1564, and 1577 MeV. We tentatively associate these five masses with the broad PDG $S_{11}(1535)$ resonance. Indeed, the mean value of our five masses, $\bar{M} \approx 1543$ MeV, is close to the PDG mean-mass value of 1535 MeV. The gap between the extreme masses, 72 MeV,

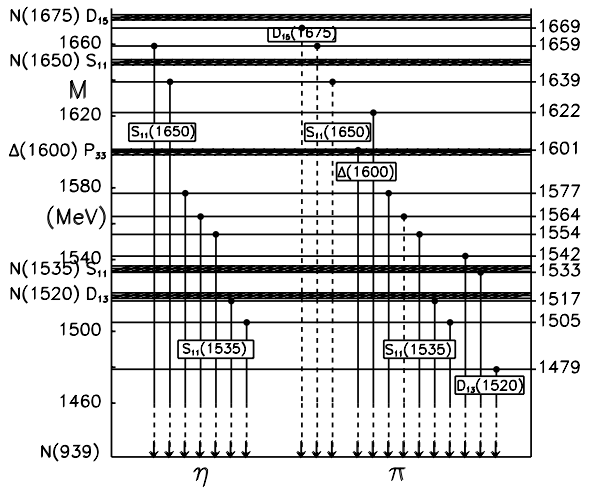

FIG. 35. Disintegration channels of the narrow baryonic resonances experimentally observed, and an attempt to associate them with broad PDG resonances.

TABLE VII. Quantitative information concerning the narrow baryonic structures extracted from the following reactions: $pp \to ppX$ [1], $pp \to p\pi^+ n$ [2], $pp \to pp\pi^0$ [3], and $pp \to pp\eta$ [4]. This information is used in Fig. 34. The masses are in MeV; the angles are in degrees.

Channel	Fig.	Reaction	T	θ	Variable	Branch	1st mass	2nd mass	3rd mass	4th mass
(a)	7	[1]	1520	0°	M_{psX}	upper	1535			
(b)	7	[1]	1520	2°	M_{psX}	upper	1482	1500	1535	1565
(c)	7	[1]	1520	5°	M_{psX}	upper	1476	1538		
(d)	7	[1]	1520	9°	M_{psX}	upper	1535	1575		
(e)	8	[1]	1805	0.75°	M_{psX}	upper	1635	1668		
(f)	8	[1]	1805	3.7°	M_{psX}	upper	1637	1669		
(g)	8	[1]	1805	6.7°	M_{psX}	upper	1667			
(h)	8	[1]	1805	0.75°	M_{pfX}	upper	1636	1666		
(i)	8	[1]	1805	3.7°	M_{pfX}	upper	1637			
(j)	8	[1]	1805	6.7°	M_{pfX}	upper	1640	1659		
(k)	8	[1]	1805	9°	M_{pfX}	upper	1641			
(l)	9	[2]	1520	0°	$M_{n\pi+}$	upper	1505	1540		
(m)	9	[2]	1520	2°	$M_{n\pi+}$	upper	1508	1545		
(n)	9	[2]	1520	5°	$M_{n\pi+}$	upper	1506	(1540?)		
(o)	9	[2]	1520	9°	$M_{n\pi+}$	upper	1508			
(p)	9	[2]	1520	13°	$M_{n\pi+}$	upper	1588			
(q)	9	[2]	1520	17°	$M_{n\pi+}$	upper	(1550?)			
(r)	10	[3]	1520	2°	$M_{ps\pi^0}$	upper	1479	1490		
(s)	11	[3]	1520	9°	$M_{ps\pi^0}$	upper	1512			
(t)	12	[3]	1520	13°	$M_{ps\pi^0}$	upper	1513.7			
(u)	12	[3]	1520	13°	$M_{pf\pi^0}$	upper	1520.5	1531.9		
(v)	13	[3]	1520	17°	$M_{ps\pi^0}$	upper	1514.2			
(w)	13	[3]	1520	17°	$M_{pf\pi^0}$	upper	1520	1531.5		
(x)	14	[3]	1520	17°	$M_{pf\pi^0}$	lower	1520	1531		
(y)	15	[3]	1805	13°	$M_{ps\pi^0}$	upper	1558	1582	1600.3	
(z)	16	[3]	1805	13°	$M_{pf\pi^0}$	upper				
(α)	3	[3]	1805	17°	$M_{ps\pi^0}$	upper	1534	1597.5		
(β)	17	[3]	1805	17°	$M_{pf\pi^0}$	upper	1601.1	1622.6		
(η)	18	[3]	1805	17°	$M_{p\pi^0}$	all	1599.5	1620.5		
(δ)	20	[4]	1520	0°	$M_{ps\eta}$	upper	1500	1519	1564	
(ϵ)	4	[4]	1520	2°	$M_{ps\eta}$	upper	1502	1519.5	1564	
(φ)	21	[4]	1520	5°	$M_{ps\eta}$	upper	1520.5	1567		
(γ)	22	[4]	1520	9°	$M_{ps\eta}$	upper	1564.2			
(χ)	23	[4]	1520	0°	$M_{pf\eta}$	lower	1561.5	1580		
(ι)	24	[4]	1520	2°	$M_{pf\eta}$	lower	1562.4	1580.1		
(π)	25	[4]	1520	5°	$M_{pf\eta}$	lower	1560.1	1576.2		
(κ)	26	[4]	1520	9°	$M_{pf\eta}$	lower	1553.1	1567		
(λ)	32	[4]	1805	0.75°	$M_{p\eta}$	all	1642.5	1656.9		
(μ)	32	[4]	1805	3.7°	$M_{p\eta}$	all	1642.3	1658.7		
(ν)	32	[4]	1805	6.7°	$M_{p\eta}$	all	1644.2	1659.8		

fills half of the estimated PDG width of 150 MeV. That several narrow-resonance baryons have an $N\eta$ disintegration channel may, eventually, agree with a calculation of the total $pp \to pp\eta$ cross section [23]. Ceci *et al*. [23] "emphasize the fact that a single resonance model, using only $N(1535)$ drastically fails to describe the experimental data. The next S_{11} resonance $N(1650)$ must be included, and the introduction of the third controversial $S_{11}N(2090)$ represents a further improvement."

The second group of masses that disintegrate through $N\pi$ and $N\eta$ modes are at $M = 1639$ and 1659 MeV. Here $\bar{M} \approx 1649$ MeV is very close to the PDG mass value of the second S_{11} resonance, which is 1650 MeV. The gap between these masses, 20 MeV, is much smaller than the PDG estimated width of 150 MeV.

B. Masses having no $N\eta$ disintegrating channel

Here again, a relatively large gap allows us to tentatively divide the masses of these narrow resonances into two groups. The first group corresponds to the following masses: 1479, 1533, and 1542 MeV. Here $\bar{M} \approx 1518$ MeV and is very close to the PDG mean mass value of the $D_{13}(1520)$ resonance. The gap between extreme masses, 63 MeV, corresponds, as in the case of $S_{11}(1535)$, to half of the estimated width of the broad PDG resonance.

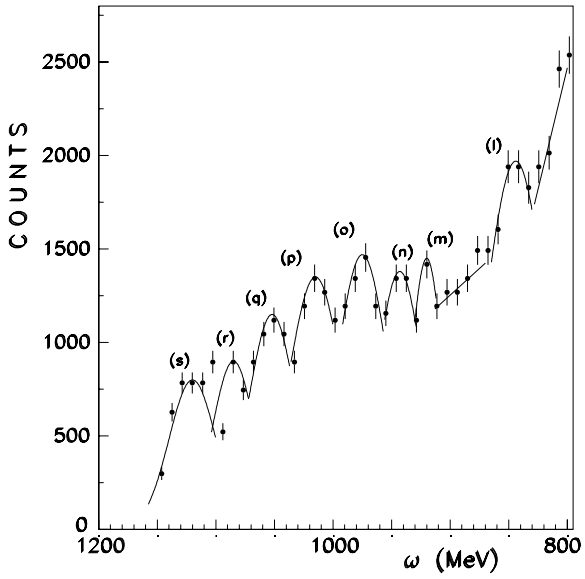

FIG. 36. The $p(\alpha, \alpha')X$ spectrum at $T_\alpha = 4.2$ GeV, and $\theta = 2^\circ$, measured at SPES4 (Saturne) [25]. Only the part of the spectrum corresponding to the baryonic mass range studied here ($1470 \leqslant M \leqslant 1680$ MeV) is shown.

The second group of masses that do not have the $N\eta$ disintegration mode corresponds to the following masses: $M = 1601$ and 1622 MeV. Here $\bar{M} \approx 1611$ MeV is close to the PDG mean mass value of the Δ $P_{33}(1600)$ resonance, which is 1600 MeV.

It appears therefore that all our masses of narrow baryonic resonances can be associated with PDG resonances, provided the latter can be split into several narrow resonances. Only one, at $M = 1669$ MeV, could be a part of the $D_{15}(1675)$ PDG resonance. However, it could also be associated with several hypothetical heavier narrow resonances, which are not observed since their masses lie outside our mass acceptance.

C. Discussion concerning the branching ratios

Since we observe narrow baryonic resonances that disintegrate into $N\pi$ and $N\eta$, it is tempting to compare the ratios of the number of events between the two channels.

The comparison between the $p\eta$ final-state data (channels δ to ν in Fig. 34) and data obtained without final-state definition (channels a to k in Fig. 34) is meaningless.

The comparison between the $p\eta$ final-state data (channels δ to ν in Fig. 34) and $n\pi^+$ final-state data (channels l to q in Fig. 34) is also meaningless. Indeed, although we have data at the same angles ($\theta = 0^\circ$ and 2°) from the same branch, namely the upper branch, for both reactions, the final states are totally different, since in one case the π^+ is detected and the neutron is slow, and in the other case, the proton is detected and the η is slow.

The comparison between the $p\eta$ final-state data (channels δ to ν in Fig. 34) and the $p\pi^0$ final state data (channels r to η in Fig. 34) is more promising. Indeed we have, in both channels, data showing a narrow peak at $M = 1517$ MeV at the same incident proton energy ($T_p = 1520$ MeV), from the same branch (the upper branch), and using the same slow proton for both reactions. However, the η is selected at small angles (from $\theta = 0^\circ$ to 2°, channels δ to ϵ in Fig. 34), when the π^0 is selected at large angles (from $\theta = 13^\circ$ to 17°, channels t to $\times$ in Fig. 34). These limitations result from the spectrometer momenta limits.

We conclude that we are unable to give relative branching ratios.

It is worthwhile to point out that a large background of two pions exist, whose branching ratios cannot be compared with the $N\pi$ or $N\eta$ branching ratios, because our mass (and angular) range is too small.

VI. COMPARISON WITH OTHER RESULTS

Occasionally data, published to study different problems, display narrow discontinuities that are not discussed by the authors. These narrow discontinuities are sometimes, but not always, well defined statistically. The authors of such results did not take into account the possibility of associating the discontinuities of their spectra with possible narrow baryonic low-mass structures. We present and discuss some such results and limit our discussion to the mass range $1.47 \leqslant M \leqslant 1.68$ GeV, which is the range studied in this work.

A. The $p(\alpha, \alpha')X$ reaction

A precise spectra of the $p(\alpha, \alpha')X$ reaction was obtained 12 years ago at SPES4 (Saturne) to study the radial excitation of the nucleon in the $P_{11}(1440$ MeV) Roper resonance. A spectrum measured at $T_\alpha = 4.2$ GeV and $\theta = 0.8^\circ$ [24] was defined in the baryonic missing-mass range $1030 \leqslant M \leqslant 1490$ MeV. A peak is extracted at $M = 1478$ MeV, which is very close to $M = 1479$ MeV where a peak extracted from our data. Another spectrum measured at $T_\alpha = 4.2$ GeV and $\theta = 2^\circ$ [25] extended to $M = 1588$ MeV. Figure 36 shows the part of this spectrum for masses larger than 1470 MeV. The statistical errors could not be larger than a factor of 2 from the those extracted using the given counts [26]. The error bars are therefore multiplied by a factor of 2. The comparison of the masses of the narrow structures extracted from the experiments performed with the SPES4 and SPES3 beam lines is shown in Fig. 37 and Table VIII. The positions of the structures observed in both experiments agree to a great extent. This agreement is obtained from published data, originally obtained from experiments with different objectives and carried out by different physicists, who used different setups, beams, and reactions.

B. Total cross sections of πN reactions

Rather old total cross sections of πN reactions were reported in a CERN compilation [27]. Whereas neither $\sigma_T(\pi^- p)$ nor σ_T $(\pi^+ p)$ [28] display any narrow peaks, the data from σ_T $(\pi p \rightarrow N\pi^0)$ [27,29] show small narrow and not very precise peaks close to M = 1500 MeV [1505], 1635 MeV [1639], and

TABLE VIII. Masses (in MeV) of narrow exotic baryons observed in SPES3 data and extracted from previous $p(\alpha, \alpha')X$ spectra measured at SPES4 [25].

SPES3 mass	1479	1505	1517	1533	1542	(1554)	1564	1577
Peak marker	(l)	(m)	(n)	(o)	(p)	(q)	(r)	(s)
SPES4 mass 2°	1477	1507	1517	1530	1544	1557	1569	1580

1660 MeV [1659]. Here the numbers in square brackets are the masses extracted in this work.

C. η meson photoproduction on the proton

The total cross section of the η meson photoproduction on hydrogen was measured near threshold at ELSA (Bonn) [30]. The very small incident photon energy range prevents the possibility of observing baryonic structures. Total and differential cross sections for the $pp \to pp\eta$ reaction were studied at the internal beam facility at COSY [31]. In this case the total range of $M_{p\eta}$ is also very restricted. The same reaction was also studied at the MAMI accelerator in Mainz [32,33]. Total-cross-section data are plotted in Fig. 38. Three small and narrow peaks (total width $\approx$ a few MeV) can be extracted, even if the definition of the second one (a2) is better than those of the two other peaks. The masses of these three peaks can be compared to the first three masses in our data, above the threshold of η meson photoproduction off the proton. These masses fit accurately with the masses extracted from the SPES3 data, as can be seen in Table IX.

The differential cross section of η photoproduction on the proton was also measured at GRAAL (Grenoble) [34]. Here again, neither the resolution (nor the binning) is appropriate for the study of narrow peaks.

D. Near-threshold electroproduction of η meson on the proton

The differential cross section of the $p(e, e'p)\eta$ reaction was studied at JLab in Hall C [35]. The η electroproduction was also studied at JLab with the CLAS spectrometer [36]. The integrated cross sections show small peaks in the vicinity of 1561, 1582, and 1621 MeV. Here again, the binning of 20 MeV prevents a better observation of any eventual narrow peak. However, the masses are close to the those extracted from the SPES3 data.

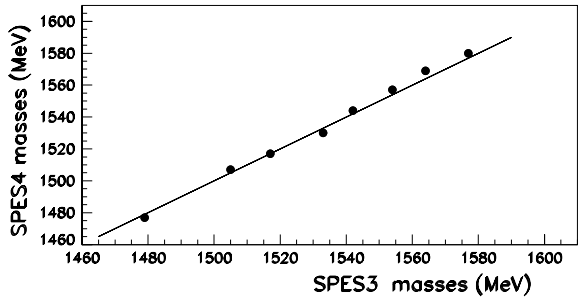

FIG. 37. Comparison of narrow mass structures observed in the SPES3 data with those extracted from the $p(\alpha, \alpha')X$ spectrum at $T_\alpha = 4.2$ GeV, and $\theta = 2°$, measured at SPES4 (Saturne) [25]. Only the part of the spectrum corresponding to the baryonic mass range studied here ($1470 \leqslant M \leqslant 1680$ MeV) is shown.

E. The $\gamma p \to n\pi^+$ reaction

Differential cross sections for the $\gamma p \to n\pi^+$ reaction were measured at the Bonn 2.5-GeV electron synchrotron [37]. The bremsstrahlung beam allows measurements over a wide incident energy range, typically $0.31 \leqslant T_\gamma \leqslant 2$ GeV, at six angles between $\theta_\pi = 180°$ and 95°. Additionnal data, in a more limited photon energy range, were taken at six outgoing pion angles between $\theta = 85°$ and 35° [38]. Figure 39 shows two small peaks extracted at $\theta = 65°$ at $M = 1.638$ GeV [$\sigma(\Gamma) = 10$ MeV] and at $M = 1.689$ GeV [$\sigma(\Gamma) = 8$ MeV]. The first of these masses is very close to one of our narrow peak masses ($M = 1639$ MeV) and the second one is a little higher than our experimental acceptance.

The differential cross section of the reaction $\gamma p \to \pi^+ n$ was measured with PHOENICS at ELSA over a large range of photon energy: $220 \leqslant E_\gamma \leqslant 900$ MeV [39]. However, the wide binning implies that any narrow peak would be washed out and thus be unobservable.

F. Meson photoproduction on the nucleon

Many cross sections were measured on the proton and neutron, with one or more pions produced. A review article lists the corresponding results [40]. Several other recent experiments were performed with a binning that precludes distinguishing narrow peaks. In the mass range studied in this work, many recent results have been obtained at the CEBAF Large Acceptance spectrometer and at other accelerators at MAMI, ELSA, and GRAAL [41] to name a few. The resolution and the binning of these data are too weak, preventing the possibility of observing narrow structures such as those shown

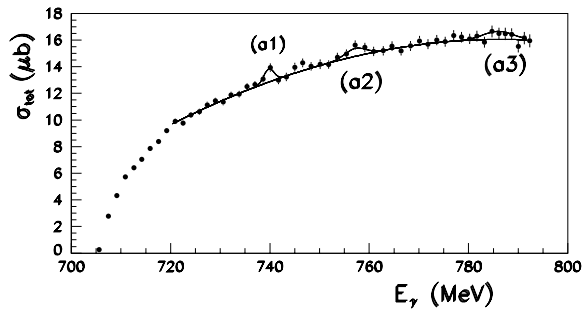

FIG. 38. Near-threshold photoproduction of the η meson on the proton. The data were taken at MAMI (Mainz) [32,33]. The quantitative information of the extracted peaks is given in Table IX.

TABLE IX. Total cross section of η meson photoproduction on the proton. Measurements were performed at MAMI [32, 33]. Small peaks (a1), (a2), and (a3) are extracted (see Fig. 38).

Peak	E_γ (MeV)	$\sqrt{(s)}$ (MeV)	SPES3 mass (MeV)
(a1)	739.8	1506	1505
(a2)	757.2	1517	1517
(a3)	786.0	1534.7	1533

previously. This is typically the case for the $\gamma p \rightarrow p\pi^0\pi^0$ total cross section measured at GRAAL.

The cross section for the reaction $ep \rightarrow e'p\pi^+\pi^-$ was measured at JLab (CLAS) in the resonance region $1.4 \leqslant W \leqslant 2.1$ GeV [42]. The authors found resonant structures that were not visible in previous experiments. The η meson electroproduction cross section was also measured at JLab (CLAS) with a center-of-mass total energy $1.487 \leqslant W \leqslant 1.635$ GeV [43]. The authors concluded that there was some indication of a Q^2 dependence of the width of the $N(1535)S_{11}$ resonance, although the data are not conclusive. They also attributed the new structure they observed at $W \approx 1.65$ GeV to an interference between S and P waves.

Photon and π^0 electroproduction from hydrogen were studied at JLab Hall A [44]. The excitation curves, presented with a binning of 20 MeV, show an oscillatory pattern of possible peaks with widths that would be much smaller than those ($\Gamma \approx 200$ MeV) of classical baryonic resonances.

Total photoabsorption cross sections were also measured at MAMI [45] in the photon energy range $200 \leqslant E_\gamma \leqslant 800$ MeV, for several target nuclei. In this last data set, the binning is smaller ($\approx$8 MeV) in the region of $M = 1.5$ GeV, but the total cross section is not the best channel for observing narrow exotic, and therefore small, effects.

VII. COMPARISON WITH MODELS OF BARYONIC RESONANCES

The classical baryonic spectrum, in the mass region studied here, was analyzed through a partial-wave analysis of pion-nucleon elastic scattering data [16] and partial-wave analyses of single-pion photoproduction data [17,18]. In both cases, the data were obtained with binnings close to 20 MeV.

The total and differential cross sections of the baryonic production in nucleon-nucleon reactions were calculated in the one-boson exchange model [46]. The authors concluded that their model results, after adjustment to the elastic nucleon-nucleon scattering, agree-with those of the experiment.

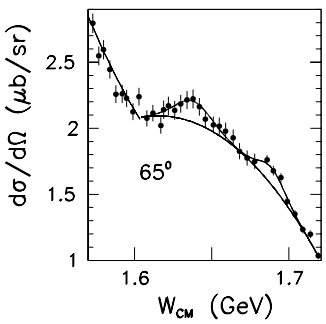

FIG. 39. Differential cross section at $\theta = 65^\circ$ of the $\gamma p \rightarrow \pi^+ n$ reaction measured at Bonn [37].

Many models of baryonic resonances have been proposed (see Ref. [4]). The quark models are restricted to the assumption of $|q^3\rangle$ wave functions, without considering additionnal $q\bar{q}$ pairs or gluonic contributions [4,47,48]. These calculations are often related to the search for "missing baryons," which possibly couple weakly to the $N\pi$ channel [49]. The low-lying baryon spectrum was calculated within the chiral constituent quark model [50]. The light-baryon spectrum was calculated within a relativistic quark model with instanton-induced quark forces [51]. On the basis of the three-particle Bethe-Salpeter equation, a good description of the overall baryonic mass spectrum up to the highest spin states was obtained [52].

The properties of baryon resonances in the mass range studied in this paper were calculated [53] using πN data and a multichannel unitary model. The authors found "results similar to previous analyses for strongly excited states, but the results can vary considerably when the states are weak." They emphasize "that the full width of the $S_{11}(1535)$ varies largely, due to the close proximity of the resonance pole to the ηN threshold." It is noteworthy that the widths found in the calculation of [54] are consistent, for the $S_{11}(1535)$, with our "experimental total" width obtained by combining the shift between the extreme masses (1505 and 1577 MeV) and the width of each narrow structure. Indeed, the calculated width in [53] for ηN is $\Gamma = 66 \pm 13$ MeV, and the calculated width for πN is $\Gamma = 77 \pm 17$ MeV.

Several recent works investigate the baryon spectroscopy in lattice QCD [55,56]. Discussion of these results lies outside the scope of the present work.

VIII. CONCLUSION

Using the SPES3 spectrometer and detection system at Saturne, the $pp \rightarrow p\pi^+X$ and $pp \rightarrow ppX$ reactions were studied at two incident energies: $T_p = 1520$ and 1805 MeV. With the help of software cuts on the missing-mass spectra, the following final states were selected: $p\pi^0$, $n\pi^+$, and $p\eta$. The $N\pi\pi$ final state contributed to the physical background. Because of the good resolution and reasonable statistics, we were able to observe a large number of narrow and well-separated peaks in the range $1.47 \leqslant M \leqslant 1.68$ GeV. In some cases the peak to background ratio is not large; therefore a peak is only considered as a narrow baryonic resonance when several peaks are extracted at the same mass ($\pm$3 MeV), and in different experimental data sets. The widths of these peaks are lower than those reported by the PDG.

We have separated the narrow states observed into two classes: those where a deexcitation into a $N\eta$ final state was observed and those where this was not the case. When combining the masses of narrow states seen in both $N\eta$ and $N\pi$ final states, we tentatively identify them as being "fine structures" of $N^*(1535)S_{11}$ and $N^*(1650)S_{11}$. In the same way, the masses not observed in the $N\eta$ final state are tentatively identified as being "fine structures" of $N^*(1520)$ and $\Delta(1600)P_{33}$. Such assumptions give, for each case, a mean mass that is in fairly good agreement with the mass of the broad PDG baryonic resonance. Such a description could

also justify the different mean masses sometimes observed when different reactions are used. For example, the mass of the $N(1535)S_{11}$ was found at $M = 1549 \pm 2$ MeV from the $\pi^- p \to \eta$p reaction [57] and at $M = 1525 \pm 10$ MeV from the $\gamma N \to \pi N$ reaction [17]. Also, the calculated partial widths are generally too small to account for the experimental values of broad PDG baryons [58].

By analogy with nuclear physics, we suggest that the previously broad PDG baryonic resonances are in fact collective states of several weakly excited and narrow resonances. These resonances can be single-particle-or-quasi-particle (from constituent quark) states, with quark structures more complicated than $|q\rangle^3$. We suggest that the reason for which these narrow, weakly excited peaks were not observed till now is due to the lack of experimental precision of previous experiments.

It is clear that these observations—if confirmed by other experiments—would be a milestone in hadron spectroscopy and would impose a big challenge to hadron theorists. The hadron structure is richer than has been often thought up till now. Its investigation requires nonpertubative methods in the mass range studied in this paper. Explaining the small widths observed remains a mystery. One possibility may be that there exists some "quark tunneling" from one quark cluster to another. It is then possible that new theoretical tools will have to be developed. Indeed, a complete description of hadrons should incorporate valence quarks, sea quarks, and gluonic degrees of freedom.

ACKNOWLEDGMENTS

We thank Professor H. Fischer for his letter saying that he, and his collaborators, were convinced that the unusual behavior of their differential cross sections are a real effect. We thank Professor B. Krusche for sending us the numerical values of η meson photoproduction and Professor H. P. Morsch for stimulating discussions.

[1] D. E. Groom *et al*. (Particle Data Group) Eur. Phys. J. C **15**, 1 (2000).
[2] H. Kamano and M. Arima, Phys. Rev. C **69**, 025206 (2004).
[3] R. M. Edelstein *et al*., Phys. Rev. D **5**, 1073 (1972).
[4] S. Capstick and W. Roberts, Prog. Part. Nucl. Phys. **45**, S241 (2000).
[5] F. Iachello, in *Proceedings of the Fourth CEBAF/INT Workshop, N^* Physics*, edited by T.-S. H. Lee and W. Roberts (1996), p. 78.
[6] A. Kiswandhi, S. Capstick, and S. Dytman, Phys. Rev. C **69**, 025205 (2004).
[7] D. Brommel, P. Crompton, C. Gattringer, L. Y. Glozman, C. B. Lang, S. Schaefer, and A. Schäfer, Phys. Rev. D **69**, 094513 (2004).
[8] E. E. Kolomeitsev and M. F. M. Lutz, Phys. Lett. **B585**, 243 (2004).
[9] C. Wilkin, Phys. Scripta **64**, 427 (2001); G. Fäldt and C. Wilkin, Nucl. Phys. **A596**, 488 (1996).
[10] B. Kämpfer, L. P. Kaptari, and A. I. Titov, *Proceedings of the International Workshop XXXII on Gross Properties of Nuclei and Nuclear Excitations, Hirschegg, Jan. 11–17, 2004*, arXiv:nucl-th/0402044.
[11] B. Tatischeff, J. Yonnet, M. Boivin, M. P. Comets, P. Courtat, R. Gacougnolle, Y. Le Bornec, E. Loireleux, M. MacCormick, F. Reide, and N. Willis, Eur. Phys. J. A **17**, 245 (2003).
[12] B. Tatischeff, J. Yonnet, M. Boivin, M. P. Comets, P. Courtat, R. Gacougnolle, Y. Le Bornec, E. Loireleux, M. MacCormick, F. Reide, and N. Willis, Surv. High Energy Phys. **19**, 55 (2004).
[13] B. Tatischeff, J. Yonnet, M. Boivin, M. P. Comets, P. Courtat, R. Gacougnolle, Y. Le Bornec, E. Loireleux, M. MacCormick, F. Reide, and N. Willis, Transworld Res. Network, Recent Res. Devel. Physics **5**, 1165 (2004); B. Tatischeff, in *Proceedings XVI International Baldin Seminar on High Energy Physics Problems, Dubna (2002)*, edited by A. N. Sissakian, V. V. Burov, and A. I. Malakhov (2004), Vol. II, p. 153.
[14] D. M. Manley and E. M. Saleski, Phys. Rev. D **45**, 4002 (1992).
[15] R. E. Cutkosky and S. Wang, Phys. Rev. D **42**, 235 (1990).
[16] R. A. Arndt, I. I. Strakovsky, and R. L. Workman, and M. M. Pavan, Phys. Rev. C **52**, 2120 (1995); D. M. Manley and E. M. Saleski, Phys. Rev. D **45**, 4002 (1992); R. E. Cutkosky and S. Wang Phys. Rev. D. **42**, 235 (1990).
[17] R. A. Arndt, I. I. Strakovsky, and R. L. Workman, Phys. Rev. C **53**, 430 (1996).
[18] R. A. Arndt, W. J. Briscoe, I. I. Strakovsky, and R. L. Workman, Phys. Rev. C **66**, 055213 (2002).
[19] R. A. Arndt, I. I. Strakovsky, R. L. Workman, and M. M. Pavan, Phys. Scripta **T87**, 62 (2000).
[20] R. A. Arndt, I. I. Strakovsky, and R. L. Workman, Phys. Rev. C **56**, 577 (1997).
[21] R. A. Arndt, A. M. Green, R. L. Workman, and S. Wycech, Phys. Rev. C **58**, 3636 (1998).
[22] In view of shortening the text, some figures are not shown when narrow structure could not be extracted. They will be shown in: B. Tatischeff, J. Yonnet, M. Boivin, M. P. Comets, P. Courtat, R. Gacougnolle, Y. Le Bornec, E. Loireleux, M. MacCormick, and F. Reide, to be sent to arXiv:nucl-ex.
[23] S. Ceci, A. Svarc, and B. Zauner, arXiv:nucl-th/0402040 (2004).
[24] H. P. Morsch *et al*., Phys. Rev. Lett. **69**, 1336 (1992).
[25] H. P. Morsch, in *Proceedings of the Dixieme Journee Thematique de l'IPN d'Orsay (1995)*.
[26] H. P. Morsch (private communication).
[27] V. Flaminio, W. G. Moorhead, D. R. O. Morrison, and N. Rivoire, CERN-HERA 83-01 Compilation (1983).
[28] A. A. Carter *et al*., Nucl. Phys. **B26**, 445 (1971).
[29] F. Bulos *et al*., Phys. Rev. **187**, 1827 (1969); Phys. Rev. Lett. **13**, 558 (1964).
[30] J. W. Price *et al*., Phys. Rev. C **51**, R2283 (1995).
[31] P. Moskal *et al*., Phys. Rev. C **69**, 025203 (2004).
[32] B. Krusche *et al*., Phys. Rev. Lett. **74**, 3736 (1995).
[33] B. Krusche *et al*., Z. Phys. A **351**, 237 (1995).
[34] F. Renard *et al*., Phys. Lett. **B528**, 215 (2002).
[35] C. S. Armstrong *et al*., Phys. Rev. D **60**, 052004 (1999).
[36] J. A. Mueller, in *Proceedings of the NSTAR 2001 Workshop*, edited by D. Drechsel and L. Tiator (World Scientific, Mainz, 2001), p. 365.

[37] H. W. Dannausen, E. J. Durwen, H. M. Fisher, M. Leneke, W. Niehaus, and F. Takasaki, Eur. Phys. J. A **11**, 441 (2001).
[38] H. M. Fisher (private communication).
[39] K. Büchler *et al*., Nucl. Phys. **A570**, 580 (1994).
[40] B. Krusche and S. Schadmand, Prog. Part. Nucl. Phys. **51**, 399 (2003).
[41] Y. Assafiri *et al*., Phys. Rev. Lett. **90**, 022201 (2003).
[42] M. Ripani *et al*., submitted to Phys. Rev. Lett., arxiv:hep-ex/0304034.
[43] R. Thompson *et al*., Phys. Rev. Lett. **86**, 1702 (2001).
[44] G. Lavessière *et al*., in *Proceedings of the NSTAR 2001 Workshop*, edited by D. Drechsel and L. Tiator (World Scientific, Mainz, 2001), (2004), p. 271.
[45] M. MacCormick *et al*., Phys. Rev. C **53**, 41 (1996).
[46] S. Huber and J. Aichelin, Nucl. Phys. **A573**, 587 (1994).
[47] S. Capstick, Phys. Rev. D **46**, 2864 (1992).
[48] N. Isgur and G. Karl, Phys. Rev. D **19**, 2653 (1979).
[49] S. Capstick and W. Roberts, Phys. Rev. D **49**, 4570 (1994).
[50] H. Garcilazo, A. Valcarce, and F. Fernandez, Phys. Rev. C **63**, 035207 (2001).
[51] U. Löring, B. Ch. Metsch, and H. R. Petry, Eur. Phys. J. A **10**, 395 (2001).
[52] B. Metsch, U. Löring, D. Merten, and H. Petry, Eur. Phys. J. A **18**, 189 (2003).
[53] S. A. Dytman, T. P. Vrana, and T.-S. H. Lee, Phys. Rep. **328**, 181 (2000).
[54] R. A. Arndt, I. I. Strakovsky, R. L. Workman, and M. M. Pavan, Phys. Rev. C **52**, 2120 (1995).
[55] D. B. Leinweber, W. Melnitchouk, D. G. Richards, A. G. Williams, and J. M. Zanotti, arXiv:nucl-th/0406032.
[56] T.-W. Chiu and T.-H. Hsieh, arXiv:hep-lat/0406016.
[57] V. V. Abaev and B. M. K. Nefkens, Phys. Rev. C **53**, 385 (1996).
[58] B. Metsch, AIP Conf. Proc. **717**, 646 (2004); arXiv:hep-ph/0403118.